

1 **High metabolic zinc demand within native Amundsen and Ross Sea phytoplankton**

2 **communities determined by stable isotope uptake rate measurements**

3 Riss M. Kell^{1,+}, Rebecca J. Chmiel¹, Deepa Rao¹, Dawn M. Moran¹, Matthew R. McIlvin¹,

4 Tristan J. Horner¹, Nicole L. Schanke³, Ichiko Sugiyama¹, Robert B. Dunbar², Giacomo R.

5 DiTullio³, Mak A. Saito¹

6 ¹Department of Marine Chemistry and Geochemistry, Woods Hole Oceanographic Institution,

7 Woods Hole, MA, USA

8 ²Doerr School of Sustainability, Stanford University, Stanford, CA 94305

9 ³Hollings Marine Laboratory, College of Charleston, Charleston, South Carolina, 29412, USA

10 *Correspondence to:* Mak A. Saito (msaito@whoi.edu)

11 ⁺Formerly published under Riss Kellogg; now affiliated with Gloucester Marine Genomics

12 Institute, Gloucester MA, 01930-3006

13 **Abstract**

14 Zinc (Zn) is an essential micronutrient for most eukaryotic phytoplankton. Zn uptake by
15 phytoplankton within the euphotic zone results in nutrient-like dissolved Zn (dZn) profiles (~~dZn~~)
16 with a large dynamic range. The combination of key biochemical uses for Zn and large vertical
17 gradients in dZn implies the potential for rapid rates of Zn removal from the surface ocean.

18 However, due to the ease of contamination at sea, direct measurements of dZn uptake within
19 natural environments have not been previously made. To investigate the demand for dZn and for
20 dissolved cadmium (dCd; a closely related nutrient-like element) within Southern Ocean

21 phytoplankton communities, we conducted ⁶⁷Zn and ¹¹⁰Cd tracer uptake experiments with
22 ~~phytoplankton communities~~ within the Amundsen Sea, Ross Sea, and Terra Nova Bay of the
23 Southern Ocean, into the >3 μm phytoplankton-particulate size fraction. The highly-productive

Formatted: Superscript

24 Amundsen Sea and Ross Sea of Antarctica host large phytoplankton blooms in the austral spring
25 and summer, during which macronutrient and micronutrient surface concentrations become
26 significantly depleted largely due to phytoplankton uptake. In autumn and winter, nutrient levels
27 are “reset” to high concentrations throughout the water column in these environments due to
28 convective overturn, advancing sea ice cover, and darkness. This annual “resetting” of nutrient
29 concentrations makes these Antarctic environments ideal locations to study the seasonal demand
30 for Zn within these productive communities.

31 We observed a high magnitude of Zn uptake ($\rho\text{Zn} > 100 \text{ pmol dZn L}^{-1} \text{ d}^{-1}$) into the
32 particulate phase that was consistent with ambient depleted dZn surface concentrations. High
33 biomass and low seawater pCO_2 appeared to exert primary control contribute to over ρZn , which
34 also in turn led to increases in ρCd likely through the upregulation of shared transport systems.
35 These high ρZn measurements further imply that only short timescales are needed to deplete the
36 large winter dZn inventory down to the observed surface levels in this important carbon-
37 capturing region. Overall, the high magnitude of Zn uptake into the particulate fraction suggests
38 that even in the Zn-rich waters of the Southern Ocean, high Zn uptake rates can lead to Zn
39 depletion and potential Zn scarcity.

40 In this study, variations in metal uptake rates over depth and time and correlations with
41 other oceanic parameters were examined. High total metal uptake rates (ρMetal) of both Zn and
42 Cd were consistent with the observed depletion of dZn and dCd surface concentrations. Our
43 findings suggest that high biomass and low seawater pCO_2 exerted primary control over
44 increasing ρZn , which in turn led to increases in ρCd likely through the upregulation of shared
45 transport systems. Overall, we observed a high magnitude of Zn uptake ($> 100 \text{ pmol dZn L}^{-1} \text{ d}^{-1}$)
46 into the particulate phase within these Southern Ocean phytoplankton communities, suggesting

Formatted: Subscript

47 ~~that even in the Zn-rich waters of the Southern Ocean, high Zn uptake rates can lead to Zn~~
48 ~~depletion and potential Zn scarcity.~~

49 **1 Introduction**

50 Zinc (Zn) is an essential trace metal micronutrient for marine phytoplankton with roles in
51 carbon fixation, organic phosphorus uptake, and transcriptional and translational processes,
52 among others (Morel et al., 2013, 2020; Shaked et al., 2006; Twining and Baines, 2013).
53 Nutrient-like depth profiles of total dissolved Zn (dZn) are characterized by depleted surface
54 concentrations due to uptake by phytoplankton within the euphotic zone, reflecting this high
55 biological demand (Fitzwater et al., 2000; Lohan et al., 2002; Middag et al., 2019; Zhao et al.,
56 2014). Zn is particularly important as a catalytic cofactor in carbonic anhydrase (CA)
57 metalloenzymes, which catalyze the reversible dehydration of HCO_3^- to CO_2 . As HCO_3^-
58 constitutes about 90% of the dissolved inorganic carbon (DIC) pool in the surface ocean, CAs in
59 marine algae are a critical part of the carbon concentrating mechanism (CCM) that maintains a
60 CO_2 supply to the carbon-fixing enzyme ribulose-1,5-biphosphate carboxylase/oxygenase
61 (RUBISCO). Less abundant divalent metal cations such as cobalt (Co^{2+}) and cadmium (Cd^{2+})
62 can replace Zn^{2+} in some algal CA subtypes (Lane et al., 2005), conferring biochemical
63 flexibility to algae confronted with low Zn bioavailability.

64 While Cd is known to cause toxic effects in most organisms (Brand et al., 1986; Das et
65 al., 1997), dCd depth profiles are also nutrient-like. As noted above, the biological use of Cd as a
66 catalytic cofactor within Cd-containing carbonic anhydrase (ζ -CA, or CDCA) likely contributes
67 to surface dCd depletion and thus to the observed nutrient-like profiles, though this remains the
68 only known biological use of Cd to date (Haas et al., 2009; Lee and Morel, 1995; Sunda and
69 Huntsman, 2000). It has also been proposed that phytoplankton may assimilate Cd abiotically—

70 this mode of Cd uptake is non-specific, a case of ‘mistaken identity’ in which phytoplankton
71 bind and store imported Cd inside the cell to avoid toxicity, coupling the cycling of Cd to the
72 biological cycle of nutrients (Horner et al., 2013). As the beneficial effect of adding Cd to
73 phytoplankton cultures has only been observed when Zn is limiting (Lee et al., 1995; Price and
74 Morel, 1990; Xu et al., 2007), it has been speculated that the ability to use Cd in place of Zn in
75 CDCA may confer a competitive advantage to Zn-limited algae under low pCO₂. To date,
76 homolog *cdca* genes have been found exclusively in diatom species (Park et al., 2007, 2008).
77 However, since the beneficial effect of Cd has also been observed in organisms such as the green
78 alga *Tetraselmis maculata* and the coccolithophore *Emiliania huxleyi* that lack the *cdca* gene
79 (Lee and Morel, 1995), it is thought that Cd may have other biochemical functions in
80 phytoplankton still awaiting discovery.

81 ~~Globally, dZn concentrations share a near-linear correlation with those of dissolved~~
82 ~~silicate (Bruland et al., 1978), a macronutrient required by diatoms to form their siliceous~~
83 ~~frustules. While this would seem to suggest that Zn is predominantly present in and~~
84 ~~remineralized simultaneously with siliceous diatom frustules at depth, this is not the case. Only a~~
85 ~~small fraction of cellular Zn (1–3%) is incorporated into frustules (Ellwood and Hunter, 2000)~~
86 ~~while the majority of Zn is instead associated with diatom organic matter (Twining et al., 2004).~~
87 ~~Furthermore, cellular Zn within sinking diatom detritus is remineralized over the same short~~
88 ~~length-scale as phosphorus (P) as opposed to the greater depths at which siliceous material~~
89 ~~remineralizes (Twining et al., 2014).~~

90 ~~Hypotheses to explain the coupling of Zn and Si generally propose that a combination of~~
91 ~~physical and biogeochemical processes (including reversible adsorption of Zn onto sinking~~
92 ~~organic particles (Weber et al., 2018)) give rise to the Zn:Si relationship, with strong Zn~~

93 ~~drawdown by Southern Ocean diatoms and the resulting export of Zn-rich biogenic particles~~
94 ~~acting as a key influence (Vance et al., 2017).~~

95 Due to the generally high (> 1nM) dZn concentrations observed in Southern Ocean
96 waters (Baars and Croot, 2011), Zn has not been considered to be a limiting micronutrient in this
97 region, despite the fact that This is complemented by the observation that Southern Ocean
98 diatom species possess cellular Zn quotas that are 3-15x higher compared to those of low-latitude
99 species (Twining and Baines, 2013), and with model-inferred Zn uptake rates used to find that
100 Southern Ocean phytoplankton account for 62% of global Zn uptake (Roshan et al., 2018). Zn is
101 rapidly stripped from Southern Ocean surface waters (Ellwood, 2008; Zhao et al., 2014)(Roshan
102 et al., 2018). This rapid removal of Zn may be, in part, due to low seawater pCO₂ resulting from
103 bloom conditions during austral summer that further exacerbates the need for inorganic carbon
104 acquisition by photosynthetic phytoplankton, which in turn exacerbates Zn demand through its
105 use as a cofactor in carbonic anhydrase (Kell et al., 2023). Ocean biogeochemical modeling
106 studies have demonstrated that model variants with high (> 4.5 mmol:mol) Zn:P uptake ratios are
107 able to reproduce the Zn-Si correlation without any explicit coupling between Zn and Si (Roshan
108 et al., 2018; de Souza et al., 2018; Vance et al., 2017), suggesting that rapid Zn removal into the
109 particulate phase is a key feature of biogeochemical cycling in the Southern Ocean.

110 Substantial removal of dZn from Southern Ocean surface waters appears associated with
111 ~~the~~ high biomass blooms and low pCO₂ conditions during austral spring and summer, and
112 ~~creat~~ing the potential for phytoplankton growth to become Zn and carbon co-limited (Kell et
113 al., 2023; Morel et al., 1994). While phytoplankton growth in the Southern Ocean is well-known
114 to be primarily limited by Fe availability (Arrigo et al., 2008; Martin, 1990), melting icebergs
115 and ice shelves are known to act as external sources of Fe (Hopwood et al., 2019; Person et al.,

116 2021; Planquette et al., 2013; St-Laurent et al., 2017) with larger Fe inputs expected from
117 increased ice melt in a warming climate. The majority of ice-melted Fe input is sourced from
118 particulate lithogenic material (entrained during grounding of ice shelves on the continent and
119 sediments). Fe in crustal material is ~~higher~~ more abundant than Zn (3.5% as Fe versus 0.0071%
120 as Zn) (Taylor and McLennan, 1985), creating a large inventory of particulate Fe available that
121 can be partially dissolved by biotic and abiotic processes. Increased dFe inputs to surface
122 Antarctic waters may act to relieve Fe stress, but would simultaneously support the development
123 of other nutrient limitations. For example, low availabilities of both dZn and vitamin B₁₂ have
124 been previously observed to co-limit phytoplankton growth with Fe in the Ross Sea (Bertrand et
125 al., 2007; Kell et al., 2023). A high demand for Zn naturally exists within eukaryotic
126 phytoplankton due to the requirement for Zn²⁺ in numerous metabolic functions; therefore,
127 without similarly enhanced inputs of dZn to the water column, the alleviation of primary Fe
128 limitation could induce Zn stress as the next most in-demand metal micronutrient. Coastal
129 polynyas that form within the Amundsen and Ross Seas during austral spring and summer are
130 particularly primed to experience Zn stress as these regions host highly productive seasonal
131 phytoplankton blooms that act as significant carbon sinks (Arrigo et al., 2012). This high
132 productivity draws pCO₂ down to low levels (< 200 ppm), putting pressure on the carbon
133 concentrating mechanism of photosynthetic phytoplankton to acquire CO₂ and thus to acquire Zn
134 as the predominantly utilized metal cofactor within carbonic anhydrases.

135 The present study enhances our knowledge of ~~what constitutes the anticipated high~~
136 ~~level~~ the rate of d-of-Zn removal from the surface Southern Ocean and uptake into the particulate
137 fraction in the Southern Ocean with empirical field data measured within native Southern Ocean
138 phytoplankton communities. This study developed a field-based, stable Zn isotope uptake rate

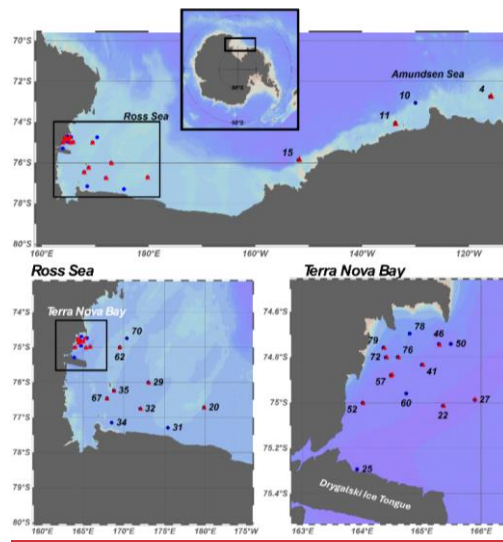
139 method, building on a prior stable Cd uptake rate method (Cox et al., 2014). While Zn uptake has
140 been measured in laboratory cultures (Sunda and Huntsman, 1992, 1995, 2000), and the
141 influence of grazing and trophic transfer studies have been conducted using radioactive isotopes
142 (Hutchins and Bruland, 1995, 1994), to our knowledge direct measurements of Zn uptake in
143 natural marine phytoplankton communities have not been conducted previously, despite interest
144 in modeling its biogeochemical uptake and cycling (Weber et al., 2018). We measured the total
145 uptake rates of Zn and Cd along the shelves of the Amundsen Sea and Ross Sea during the
146 austral summer of 2017-2018 (December – March). This was accomplished by introducing ^{67}Zn
147 and ^{110}Cd (with natural abundances of 4.10% and 12.5%, respectively) into short-term (24 hr)
148 incubation experiments. The aim was to quantify the transfer of dissolved $^{110}\text{Cd}^{2+}$ and $^{67}\text{Zn}^{2+}$ into
149 the particulate fraction exceeding 3 μm . Both stable isotopes can be used as uptake tracers by
150 analysis of isotope abundances that deviate from natural abundances within the particulate phase.
151 The transfer of added isotopes into the particulate phase is the combined result of 1) active
152 transport of metal into cells, 2) nonspecific metal adsorption to cell surfaces, 3) metal adsorption
153 to non-living particulate organic matter, and 4) metal adsorption to particulate inorganic matter,
154 though we expect active transport into cells to dominate the measured particulate isotopic signal
155 due to the high abundance of actively growing autotrophic cells in the photic zone observed in
156 the Southern Ocean during austral summer. These measurements of uptake rates were then used
157 to infer timescales of surface dZn and dCd depletion in these Antarctic environments. These
158 uptake rates contribute to understanding the biological demand and potential for Zn limitation of
159 primary productivity in highly productive coastal environments, such as the polynyas
160 surrounding Antarctica (Kell et al., 2023).

161

162 **2 Materials and methods**

163 **2.1 Study area and sample collection**

164 Samples were collected during the CICLOPS (Cobalamin and Iron Co-Limitation of
165 Phytoplankton Species) expedition (NBP18-01) aboard the RVIB *Nathaniel B. Palmer*,
166 December 11, 2017 – March 3, 2018 in the Amundsen Sea and Ross Sea of the Southern Ocean
167 (Fig. 1).



168 **Figure 1.** Map showing the stations sampled over the course of the CICLOPS cruise. Stations
169 marked by red triangles indicate those at which stable ⁶⁷Zn and ¹¹⁰Cd uptake rate experiments
170 were performed. An expanded map of stations sampled in the Ross Sea is shown at bottom left,
171 while a further expansion of stations sampled in Terra Nova Bay is shown at bottom right.
172
173

174 Station metadata is given in Table S1. Water samples were collected using trace metal clean
175 (TMC) sampling protocols described previously (Cutter and Bruland, 2012). A TMC rosette
176 suspended on a Kevlar line and equipped with twelve 8L X-Niskin bottles (Ocean Test
177 Equipment) was used to collect seawater at depths ranging from 10 – 600 m. Continuous

Formatted: Font: Not Bold

Formatted: Superscript

Formatted: Superscript

Formatted: Font: Not Bold

Formatted: Indent: First line: 0"

178 underway measurements of pCO₂ ~~measurements~~ at ~5 m depth were taken using a pCO₂
179 measurement system from Lamont-Doherty Earth Observatory (LDEO, 0.017/sec rate).
180 Hydrography data were collected using sensors deployed on a titanium trace metal rosette
181 (TMR) in tandem with TMC niskin bottles. The TMR was equipped with sensors to measure
182 temperature, conductivity, pressure, dissolved oxygen, chlorophyll (Chl) fluorescence, altimetry,
183 beam transmission, and photosynthetically active irradiance (PAR). Chl fluorescence was
184 measured using a WetLabs ECO-FL fluorometer. A complete data report and sensor list are
185 available at [NBP1801DATA.pdf \(rvdata.us\)](#). Mixed layer depth (MLD) was determined for each
186 station within Terra Nova Bay as the first depth at which the difference between the potential
187 density (σ_θ) and reference density (the potential density at 10m, σ_{ref}) was greater than or equal to
188 0.125 kg m⁻³ (Bishop and Wood, 2009; Ohnemus et al., 2017).

189 **2.2 Preparation of plasticware**

190 Polyethylene and polycarbonate sampling and incubation bottles were rigorously cleaned
191 to remove trace metal contaminants before use. Bottles were rinsed with Milli-Q water
192 (Millipore), soaked for 72h in <1% Citranox detergent, rotated, soaked for an additional 72h, and
193 then rinsed five times with Milli-Q water. Bottles were then filled with 10% HCl (Baker instra-
194 analyzed) by volume and soaked for a minimum of one week, rotated, and soaked for another
195 week. Bottles were then rinsed five times with dilute acid (HCl, pH 2) and stored double-bagged
196 in plastic zip bags. All cleaning work was conducted in a Class 100 clean room. Polypropylene
197 15 mL centrifuge tubes used in sample processing were cleaned of potential metal contamination
198 by soaking in 10% HCl for 5 days and rinsing with pH 2 HCl prior to use.

199 **2.3 Sampling for total dissolved metal analyses ~~Analyses of total dissolved Cd and Zn using~~**
200 **isotope dilution**

201 Samples for the analysis of total dissolved Zn, Cd, Fe, Mn, Cu and Ni concentrations
202 were collected shipboard by pressure-filtering X-Niskin bottles through an acid-washed 142mm,
203 0.2µM Supor membrane filter (Pall) within 3 hours of rosette recovery using high purity
204 (99.999%) N₂ gas. Total dissolved water samples were collected into 250 mL TMC polyethylene
205 bottles and ~~were~~ stored double-bagged in plastic zip bags. Seawater samples for ¹¹⁰Cd and ⁶⁷Zn
206 stable isotope uptake experiments were collected in the same way but without filtering. All
207 sample collection occurred shipboard within a TMC van containing laminar flow hoods and
208 plastic sheeting. Samples for total dissolved metal analysis were acidified to pH 1.7 with high
209 purity HCl (Optima, Fisher Scientific) within 7 months of sampling and were stored acidified at
210 room temperature for over 1 year prior to analysis.

211 **2.4 Analyses of total dissolved metals using isotope dilution**

212 Quantification of dissolved metals in samples and reference seawater was performed for
213 total dissolved Fe, Ni, Cu, Zn, and Cd using isotope dilution. 15 mL of acidified seawater sample
214 was spiked with 50 µL of a stable isotope spike solution artificially enriched in ⁵⁷Fe, ⁶¹Ni, ⁶⁵Cu,
215 ⁶⁷Zn, and ¹¹⁰Cd (*'spike isotopes'*).- *Reference isotopes used in this study were ⁵⁶Fe, ⁶⁰Ni, ⁶³Cu,*
216 *⁶⁶Zn, and ¹¹⁴Cd.* All *spike stable* isotopes were received in solid form (Oak Ridge National
217 Laboratory). Initial dissolution and all subsequent dilutions were made using concentrated nitric
218 acid (Optima, Fisher Scientific). Concentrations and ratios of isotopes for each metal in the spike
219 solution were verified by inductively coupled plasma mass spectrometry (ICP-MS) using a
220 multi-element standard curve (SPEX CertiPrep). The composition of the isotope spike addition
221 was made such that the target isotope ratios in the total, 15mL spiked sample would be ⁵⁷Fe/⁵⁶Fe
222 = 0.7, ⁶¹Ni/⁶⁰Ni = 0.5, ⁶⁵Cu/⁶³Cu = 1, ⁶⁷Zn/⁶⁶Zn = 0.7, and ¹¹⁰Cd/¹¹⁴Cd = 1 and were verified with
223 ICP-MS. These ratios were chosen to minimize the uncertainty introduced by error propagation

Formatted: Font: Bold

Formatted: Font: Bold

Formatted: Indent: First line: 0"

224 through the isotope dilution equation (Kato et al., 1990; Rudge et al., 2009; Tan et al., 2020; Wu
225 and Boyle, 1998). The same spike solution was used to spike all samples from all depths.
226 Because it is monoisotopic, total dissolved Mn was calculated using a modified isotope dilution
227 equation:

$$228 \quad \text{Mn (nM)} = \frac{{}^{55}\text{Mn}_{\text{sp}} (\text{cps})}{{}^{57}\text{Fe}_{\text{sp}} (\text{cps})} * {}^{57}\text{Fe}_{\text{spike}} (\text{nM}) * {}^{57}\text{Fe}_{\text{slope}} (\text{cps/ppb}) * \frac{1}{{}^{55}\text{Mn}_{\text{slope}} (\text{cps/ppb})} \quad (1)$$

229 in which ${}^{55}\text{Mn}_{\text{sp}}$ and ${}^{57}\text{Fe}_{\text{sp}}$ refer to the blank corrected counts per second (cps) of ${}^{55}\text{Mn}$ and ${}^{57}\text{Fe}$
230 in the spiked sample, ${}^{57}\text{Fe}_{\text{spike}}$ is the concentration of ${}^{57}\text{Fe}$ in the spike, ${}^{57}\text{Fe}_{\text{slope}}$ is the slope of
231 the external standard calibration curve (SPEX curve) relating ${}^{57}\text{Fe}$ cps to ppb, and ${}^{55}\text{Mn}_{\text{slope}}$ is the
232 slope of the external calibration curve (SPEX curve) relating ${}^{55}\text{Mn}$ cps to ppb. Due to the
233 acidification of seawater prior to ICP-MS analysis, Mn ICP-MS measurements do not include
234 contributions from humic-type Mn(III)-ligand complexes (Oldham et al., 2021). Until the
235 inclusion of Mn(III) is resolved and intercalibrated, we report these Mn values as Mn(II) and
236 note that they are consistent with prior studies employing the same acidification technique
237 (Gerringa et al., 2020; Noble et al., 2013; Sedwick et al., 2000).

238 Preconcentration of spiked seawater samples for total dissolved metal analysis was
239 performed using the automated solid phase extraction system seaFAST-pico (Elemental
240 Scientific) in offline concentration mode with an initial volume of 15 mL and elution volume of
241 500 μL (Bown et al., 2017; Jackson et al., 2018; Rapp et al., 2017; Wuttig et al., 2019). The
242 seaFAST contains a Nobias-chelate PA1 resin column (ethylenediaminetriacetate and
243 iminodiacetate) suitable for the simultaneous preconcentration of several trace metals (Fe, Mn,
244 Zn, Cu, Co, Cd, Ni) with high sensitivity and quantitative recovery (Biller and Bruland, 2012;
245 Sohrin et al., 2008). Adjusted seaFAST software settings were a 17 second load loop time and a
246 single 10 mL load cycle. ~~Process blanks consisted of pH 2 HCl (Optima, Fisher Scientific) and~~

247 ~~were processed as samples to account for any contamination introduced by instrument~~
248 ~~processing.~~

249 Reagents consisted of a 1.5M ammonium acetate pH 6.0 buffer made using glacial acetic
250 acid and ammonium hydroxide (20-22%) of the highest purity (Optima, Fisher Chemical), a 1%
251 nitric acid rinse solution (Optima grade, Fisher Chemical), and a 10% nitric acid elution buffer
252 (Optima grade, Fisher Chemical) with 10 ppb indium (¹¹⁵In, SPEX CertiPrep) added as an
253 internal standard. Solutions were prepared with 18.2 Ω Milli-Q water (Millipore). ~~Polypropylene~~
254 ~~15 mL centrifuge tubes used in sample processing were cleaned of potential metal contamination~~
255 ~~by soaking in 10% HCl for 5 days and rinsing with pH 2 HCl prior to use.~~

256 Following offline seaFAST preconcentration, multi-elemental quantitative analysis was
257 performed using an iCAP-Q inductively coupled plasma-mass spectrometer (Thermo Scientific).
258 To minimize oxide interference on metal isotopes, a cooled spray chamber and helium collision
259 gas were employed. Analytes were measured in single quadrupole mode (kinetic energy
260 discrimination [KED]). Concentrations of Mn, Fe, Ni, Cu, Zn and Cd were determined using a
261 six-point external standard curve of a multi-element standard (SPEX CertiPrep), diluted to range
262 from 1-10 ppb in 5% nitric acid. An indium standard (SPEX CertiPrep) was similarly added to
263 these standard stocks, diluted to range 1-10 ppb. Instrument injection blanks consisted of 5%
264 nitric acid in Milli-Q. Standard curve R² values were ≥ 0.98 for all metals monitored. Method
265 accuracy and precision were assessed using the 2009 GEOTRACES coastal surface seawater
266 (GSC) standard (n = 8; [Table S23](#)), which produced values consistent with consensus results.

267 2.5 Procedural blanks and limit of detection (LOD).

268 ~~Procedural blanks were quantified by preconcentrating 30mL of MilliQ water adjusted to~~
269 ~~pH 2 with HCl (Optima, Fisher Scientific) to 1mL. Metal concentrations were determined using~~

Formatted: Font: Not Bold

an external SPEX multi-element standard as described above. The LOD was calculated as 3 x the standard deviation of the blank measurements (13.5 pM Fe, 2.9 pM Ni, 1.6 pM Cu, 38.1 pM Zn, and 0.3 pM Cd).

2.6 Uptake experiments: ⁶⁷Zn and ¹¹⁰Cd spiking, incubation, and sample collection

⁶⁷Zn and ¹¹⁰Cd and stable isotope uptake experiments were modeled after those conducted by Cox et. al. 2014, with the addition of Zn uptake measurements. An overall schematic detailing these experiment workflows is shown in Fig. 2.

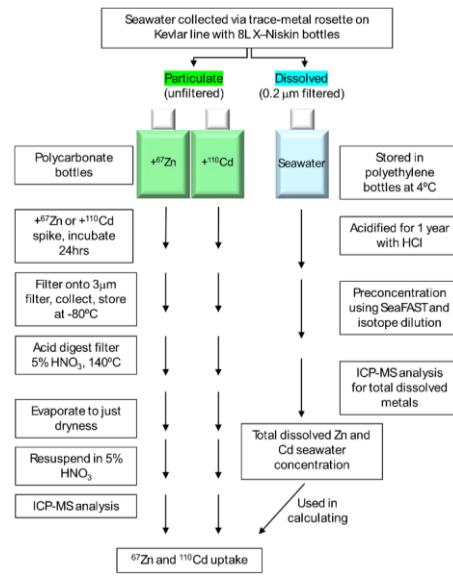


Figure 2. Diagram showing the overall workflow used to measure particulate uptake of ¹¹⁰Cd and ⁶⁷Zn and total dissolved Cd and Zn, after Cox et al. 2014.

Uptake experiments were performed at 18 stations total (Fig. 1). Raw (unfiltered) seawater was collected shipboard over a depth range of 10 – 600 m into 250 mL TMC

Formatted: Font: Not Bold

Formatted: Font: Not Bold

285 polycarbonate incubation bottles. All incubation bottles were filled with minimal headspace such
286 that the total culture volume was ~275 mL. Two incubation bottles per depth were filled with
287 raw seawater— one was spiked with ^{67}Zn , the other was spiked with ^{110}Cd . The Cd and Zn
288 isotope spikes were prepared by dissolving ^{110}CdO and ^{67}ZnO (Oak Ridge National Laboratory)
289 in 5% HNO_3 (Seastar Baseline) and were diluted using Milli-Q water to minimize added acidity.
290 When added to the filled incubation bottles, the total added (spiked) concentration of Cd was 300
291 pM and the total added concentration of Zn was 2 nM. The chosen total added concentrations
292 were based on the surface ratio of total dissolved Cd (dCd) to total dissolved Zn (dZn) reported
293 previously for the Ross Sea (Fitzwater et al., 2000). Immediately after spiking, incubation bottles
294 were sealed, inverted to mix, and transferred to flow-through on-deck incubators for 24hr.
295 Incubators were shielded by black net neutral density screening to allow 20% ambient light
296 penetration.

297 Biomass was collected after 24hr by vacuum filtering the entire volume of each
298 incubation sample at 34.5 kPa (5 psi) onto an acid-cleaned $3\mu\text{m}$, 50mm acrylic copolymer
299 (Versapore) filter (Pall) mounted on an acid-cleaned Teflon (Savillex) filtration rig. Samples
300 were filtered through $3\mu\text{m}$ pore-size filters rather than $0.2\mu\text{m}$ in order to minimize filtration
301 time (and thus time exposed to potential contamination) and to capture the bulk of eukaryotic
302 phytoplankton biomass typically found in the Southern Ocean. An aliquot of 1 mL of $0.2\mu\text{m}$
303 filtered surface seawater (collected at 10 m depth) was used to rinse the sample before collecting
304 the filter into an acid-cleaned 2 mL cryovial using acid-rinsed plastic forceps. Filter blanks were
305 duplicate $3\mu\text{m}$ acid-clean Versapore (Pall) filters that were placed onto the filtration rig, rinsed
306 with filtered surface seawater, collected, stored, and processed as samples were to correct for any
307 contaminating metals present on the filters themselves. Blanks were collected at each station.

308 Filters were stored frozen at -80 °C in acid-cleaned cryovials until analysis. The filtration rig was
309 rinsed with pH 2 HCl between samples. Polycarbonate incubation bottles were cleaned between
310 stations with a 10% HCl rinse and several rinses in Milli-Q water, followed by a brief soak in
311 10% HCl followed by a pH 2 HCl rinse. All spike addition and sample filtration procedures were
312 completed in a fabricated shipboard positive-pressure clean room environment made of laminar
313 flow hoods and plastic sheeting.

314 We note that the total Zn and Cd uptake rate values presented in this study represent
315 potential uptake rates rather than true uptake rates—this naturally arises as a consequence of
316 adding the spiked tracer ⁶⁷Zn and ¹¹⁰Cd into raw surface seawater. As this seawater is naturally
317 depleted in both metals, the spike addition artificially increases the total Zn and Cd present and
318 thus could perturb the response of biology to these additions. It should also be noted that both
319 ⁶⁷Zn and ¹¹⁰Cd spikes were not equilibrated with natural seawater before their addition to
320 incubation bottles to maintain experimental consistency. Experiments of this nature have been
321 conducted previously using radioisotopes as tracers (Cullen et al., 1999; Hutchins et al., 1999;
322 Morel et al., 1994; Sunda and Huntsman, 1995), though we chose to use stable isotopes for ease
323 of shipboard use and waste disposal.

324 **2.7 Filter digestion and particulate ICP-MS analysis**

325 All work was performed in a Class 100 clean room under laminar flow hoods. Sample
326 filters were retrieved from storage at -80 °C, removed from cryovials using plastic acid-washed
327 forceps, and transferred into trace metal clean 15 mL PFA vials with 4 mL of 5% HNO₃
328 (Optima) containing a 1 ppb Indium (In) internal standard. Filters were digested for ~3.5h at 140
329 °C using a HotBlock® heating block (Environmental Express, USA). Filters were then removed
330 and discarded, leaving behind the liquid extract. After evaporating the remaining solution to just

331 dryness, the residue was resuspended in 2 mL of 5% HNO₃ (Optima) by light vortexing. Process
 332 blank filters were digested and processed as sample filters were. Digests were analyzed in
 333 duplicate by ICP-MS using a Thermo ICP-Q plasma mass spectrometer calibrated to a multi-
 334 element standard curve (~~Spex-SPEX~~ Certiprep) over a range of 1 – 20 ppb. Duplicate values
 335 were in good agreement (Supplementary File 1), and the average value was used in further
 336 Natural calculations. Natural Cd and Zn isotope abundances of the standards were assumed to
 337 calculate concentrations of ¹¹⁰Cd, ¹¹¹Cd, ¹¹⁴Cd, ⁶⁷Zn, ⁶⁶Zn, and ⁶⁸Zn. Digests were analyzed in
 338 KED mode after an 85s sample uptake window and element mass windows were scanned 3 times
 339 during measurements. The 1 ppb In internal standard was used to correct for variation in sample
 340 delivery and plasma suppression between samples. Process blanks were subtracted from
 341 measured sample concentrations. Phosphorus concentrations were simultaneously measured by
 342 ICP-MS and were calibrated to a standard curve ranging from 100 – 3,200 ppb using a 1 ppm
 343 certified P stock (Alfa Aesar Specpure). Equation #2 was used for the calculations described
 344 above:

$$M_{particulate} = \left[\frac{M_{sample}}{In_{sample}} - \frac{M_{blank}}{In_{blank}} \right] * \frac{In_{digestion}}{M_{slope}} * \frac{V_{digested}}{V_{filtered}} \quad (2)$$

$$M_{particulate} = \left[\frac{M_{sample}}{In_{sample}} - \frac{M_{blank}}{In_{blank}} \right] * \frac{In_{digestion}}{M_{slope}} * \frac{V_{digested}}{V_{filtered}} \quad (2)$$

347 where $V_{filtered}$ is the total spiked sample volume estimated to have passed through the filter (275
 348 mL), $V_{digested}$ is the final volume the sample was resuspended in (2.0 mL), M_{sample} is the metal of
 349 interest measured in the sample in units of counts per second (cps), M_{blank} is the metal of interest
 350 measured in the process blanks (cps), M_{slope} is the slope of the metal of interest obtained by the
 351 standard curve (cps ppb⁻¹), In_{sample} is the In measured in the sample (cps), In_{blank} is the In
 352 measured in the process blanks (cps), $In_{digestion}$ is the cps of In measured in the 5% HNO₃+1 ppb

353 In digestion solution, and the calculated concentration of the metal of interest ($M_{\text{particulate}}$) is in
354 ppb ($\mu\text{g L}^{-1}$). This equation is the same as that used by Noble et. al. 2013 for the determination
355 of particulate metal concentrations using ICP-MS (Noble et al., 2013).

356 The Zn spike and Cd spike were also analyzed by ICP-MS using a tenfold dilution of
357 spike solution into 5% HNO_3 containing 1 ppb In to determine isotopic compositions and
358 concentrations. When added to filled incubation bottles (275 mL total volume), the added
359 concentrations were 288 pM ^{110}Cd , 4.51 pM ^{111}Cd , and 1.69 pM ^{114}Cd for Cd spiked bottles, and
360 were 1.91 nM ^{67}Zn , 0.045 nM ^{66}Zn , and 0.047 nM ^{68}Zn for Zn spiked bottles (Table S32). For all
361 stations and all depths, ^{67}Zn and ^{110}Cd spike concentrations exceeded natural dissolved ^{67}Zn and
362 ^{110}Cd concentrations, estimated by multiplying the total dissolved Zn and Cd by the natural
363 isotope abundance of ^{67}Zn and ^{110}Cd (0.0410 and 0.1249, respectively; see comparisons in Fig.
364 S2).

Formatted: Font: Not Bold

Formatted: Font: Not Bold

365 **2.8 Calculating zinc and cadmium uptake using ^{67}Zn and ^{110}Cd**

366 Total Zn and Cd uptake was calculated using Eq. (3) and Eq. (4), respectively. $^{110}\text{Cd}_{\text{Sample}}$
367 and $^{67}\text{Zn}_{\text{Sample}}$ are the particulate ^{110}Cd and ^{67}Zn measured by ICP-MS analysis of the 3 μm
368 sample filter (using the digestion protocol described in ~~the prior~~ section 2.7) normalized to the
369 total culture volume (275 mL) and 24 hr of incubation. $^{110}\text{Cd}_{\text{Sample}}$ and $^{67}\text{Zn}_{\text{Sample}}$ already in the
370 particulate fraction (that is, the pCd and pZn that existed in the water column upon collection of
371 the raw seawater samples) were accounted for by subtracting these pre-existing particulate ^{110}Cd
372 and ^{67}Zn values, $^{110}\text{Cd}_{\text{PEP}}$ and $^{67}\text{Zn}_{\text{PEP}}$. The pre-existing particulate value for ^{110}Cd was obtained
373 from incubation bottles that had Zn added, but no Cd spike. Likewise, the pre-existing particulate
374 value for ^{67}Zn was obtained from incubation bottles that had Cd added, but no Zn spike. The
375 ^{67}Zn spike solution was confirmed to contain virtually no ^{110}Cd , ^{111}Cd , nor ^{114}Cd . The ^{110}Cd

376 spike was likewise confirmed to contain virtually no ^{67}Zn , ^{64}Zn , nor ^{66}Zn . As a result, we
 377 assumed that the added ^{67}Zn spike did not affect the pre-existing Cd, nor did the ^{110}Cd spike
 378 affect the pre-existing Zn. It is assumed that the pre-existing particulate blank was in steady
 379 state, i.e. that it represented the Cd or Zn already in the particulate fraction and that any possible
 380 natural uptake that could occur during incubation for 24 h was negligible. The total dissolved
 381 pool of each metal isotope (denominator of each equation) is the sum of the dissolved ^{110}Cd or
 382 ^{67}Zn added as the spike ($^{110}\text{Cd}_{\text{Spike}}$, $^{67}\text{Zn}_{\text{Spike}}$) plus the natural, pre-existing dissolved ^{110}Cd or ^{67}Zn
 383 that was in the raw seawater ($^{110}\text{Cd}_{\text{Natural}}$, $^{67}\text{Zn}_{\text{Natural}}$) collected at each depth. To calculate
 384 $^{110}\text{Cd}_{\text{Natural}}$ and $^{67}\text{Zn}_{\text{Natural}}$, the total dissolved Cd or Zn measured by isotope dilution-ICP-MS
 385 (Cd_{Total} , Zn_{Total}) was multiplied by the natural abundance of ^{110}Cd and ^{67}Zn (12.49% and 4.10%,
 386 respectively). Dividing the particulate ^{110}Cd and ^{67}Zn by the total dissolved ^{110}Cd and ^{67}Zn yields
 387 the fraction of these metal isotopes that moved from the dissolved pool to the particulate pool per
 388 day (equation 3 and equation 4, respectively):

389
$$\text{Cd}_{\text{total}} \text{ Uptake Rate (pmol L}^{-1} \text{ d}^{-1}) = \frac{[^{110}\text{Cd}_{\text{Sample}} \text{ (pmol L}^{-1} \text{ d}^{-1}) - ^{110}\text{Cd}_{\text{PEP}} \text{ (pmol L}^{-1} \text{ d}^{-1})]}{[^{110}\text{Cd}_{\text{Spike}} \text{ (pmol L}^{-1}) + ^{110}\text{Cd}_{\text{Natural}} \text{ (pmol L}^{-1})]} \times \text{Cd}_{\text{total}} \text{ (pmol L}^{-1}) \text{ (3)}$$

390
$$\text{Zn}_{\text{total}} \text{ Uptake Rate (pmol L}^{-1} \text{ d}^{-1}) = \frac{[^{67}\text{Zn}_{\text{Sample}} \text{ (pmol L}^{-1} \text{ d}^{-1}) - ^{67}\text{Zn}_{\text{PEP}} \text{ (pmol L}^{-1} \text{ d}^{-1})]}{[^{67}\text{Zn}_{\text{Spike}} \text{ (pmol L}^{-1}) + ^{67}\text{Zn}_{\text{Natural}} \text{ (pmol L}^{-1})]} \times \text{Zn}_{\text{total}} \text{ (pmol L}^{-1}) \text{ (4)}$$

391 **2.9 Nutrient analyses**

392 Seawater samples taken for macronutrient analysis were filtered through 0.2 μm Supor
 393 (Pall) membrane filters and frozen at sea in acid-washed 60-mL high-density polyethylene
 394 (HDPE) bottles until analysis. Nutrient analyses were conducted by nutrient autoanalyzer by Joe
 395 Jennings at Oregon State University using previously described methods (Noble et al., 2012).

396 **2.10 Statistics and plotting**

397 Dissolved ecological stoichiometries were obtained from the slopes of two-way (type II)
 398 least squares linear regressions performed using the script lsqfitma.m rewritten from MATLAB

399 to Python by Rebecca Chmiel (<https://github.com/rebecca-chmiel/GP15>). A correlation matrix of
400 various parameters measured during NBP18-01 was created with SciPy v1.5.2 using the
401 `'scipy.stats.pearsonr'` function, yielding Pearson correlation coefficients and p values that were
402 visually represented using Seaborn v.0.11.1 and Matplotlib v3.3.2. Ocean sections were plotted
403 using Ocean Data View v5.3.0 with gridded bathymetry file ETOPO1_2min. Outliers (see Data
404 Availability) were excluded from ocean sectional plots. Mixed layer depth was calculated using
405 the potential density function (pden) within the python-seawater module (v3.3.4). Depth-
406 integrated uptake rates were calculated using the 'auc' function within the Scikit-learn (v0.23.2)
407 Python library. Figures were made using matplotlib (v3.3.2), Ocean Data View (v5.5.2), Excel
408 (2019), and RStudio (v1.3.1093). ODV color palettes (<https://doi.org/10.5281/zenodo.1243862>)
409 are inverse 'roma' for trace metal and macronutrient concentrations, 'thermal' for Zn and Cd
410 uptake rates, and 'algae' for total fluorescence (Cramer, 2023).

411 3 Results

412 3.1 Amundsen Sea

413 Zn and Cd uptake rate experiments were conducted at 18 stations. We define 3 groups of
414 stations based on location: the Amundsen Sea, Ross Sea, and Terra Nova Bay (TNB) groups
415 (Fig. 1). Uptake rates were assessed at 3 stations (4, 11 and 15) within the Amundsen Sea group,
416 6 stations (20, 29, 32, 35, 62, and 67) within the Ross Sea group, and 9 stations (22, 27, 41, 46,
417 52, 57, 72, 76 and 79) within the TNB group spanning ~10 – 250 m depth for a total of 18
418 stations and 125 samples. An overall schematic detailing these experiment workflows is shown
419 in Fig. 2. The experimental design was validated by comparison of surface particulate ^{67}Zn : ^{68}Zn
420 and ^{110}Cd : ^{114}Cd ratios measured in spiked samples with with natural abundance ratios
421 measured in control (unspiked) samples. Samples spiked with ^{67}Zn had particulate ^{67}Zn : ^{68}Zn

Formatted: Font: Not Bold

Formatted: Font: Not Bold

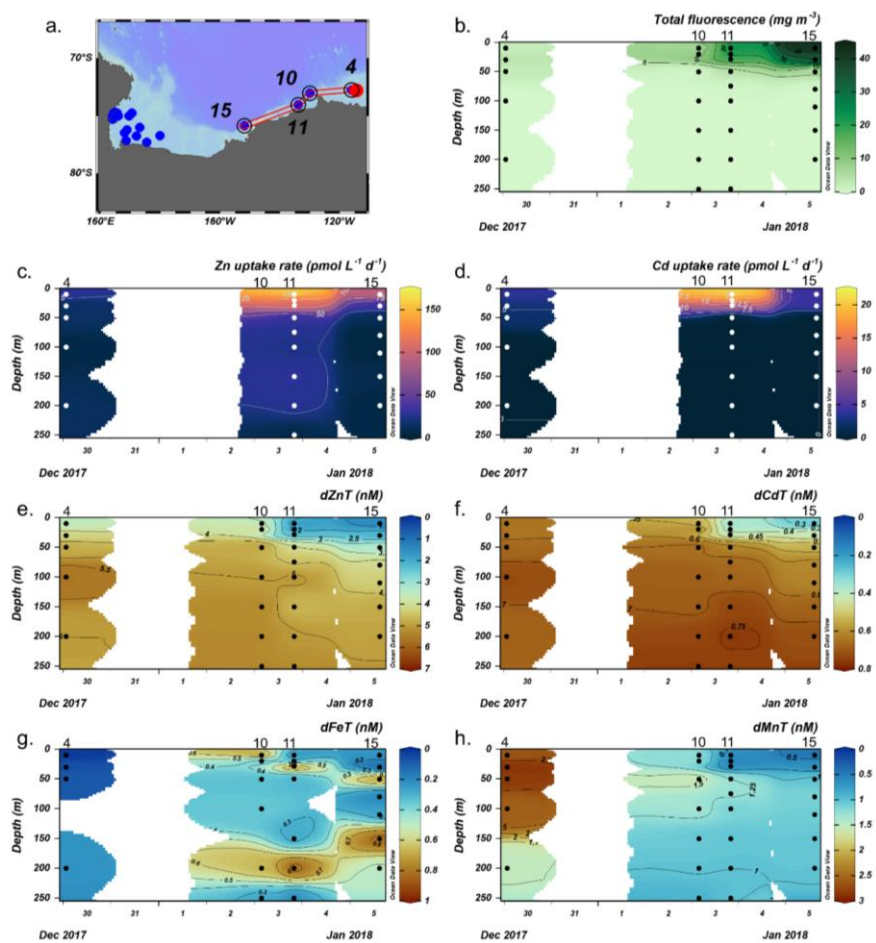
422 ratios larger than natural abundance ratios at all stations (as was also true for ^{110}Cd spiked
423 samples and Cd natural abundances; Fig. S1), indicative of uptake of the spike into the
424 particulate phase.

425 The Amundsen Sea stations represented a linear cruise track, and we report total
426 dissolved metal concentrations ($d\text{Metal}_T$) and uptake rates (ρMetal) over time in order of station
427 sampling date (Fig. 3a).

428
429

Formatted: Font: Not Bold

Formatted: Font: Not Bold



430
 431 **Figure 3.** Total fluorescence and trace metal concentrations measured at Amundsen Sea stations
 432 shown over time. (a) Map showing station locations, (b) total chlorophyll (Chl) fluorescence, (c)
 433 total Zn uptake rates, (d) total Cd uptake rates, (e) total dissolved Zn, (f) total dissolved Cd, (g)
 434 total dissolved Fe, and (h) total dissolved Mn measured in the upper 250 m represented in color
 435 scale. Uptake experiments were not performed at station 10. Metal concentrations measured to
 436 500 m depth are shown in Figure S3. dZnT, total dissolved Zn; dCdT, total dissolved Cd; dFeT,
 437 total dissolved Fe; dMnT, total dissolved Mn.
 438

439 Among these stations, total Chl fluorescence was lowest at station 4 and increased

440 moving westward along the transect to a Chl maximum of 41.8 mg m^{-3} at station 15, 10 m (Fig.

Formatted: Font: Not Bold

441 3b). Maximum surface concentrations of dZn, dCd and dMn were highest at station 4 (3.5 nM,
442 639 pM, and 2.6 nM at 10 m, respectively; Fig. 3e, f, h), likely reflecting the relatively smaller
443 amount of total biomass (as indicated by total Chl fluorescence; Fig. 3b) at this station.
444 Concentrations of dZn, dCd and dMn decreased moving westward along the transect (Fig. 3e, f,
445 h) as total Chl fluorescence increased (Fig. 3b). Total Zn uptake rates (ρZn) and total Cd uptake
446 rates (ρCd) were highest at station 11 (158 and 21 pmol L⁻¹ d⁻¹, respectively, at 10 m; Fig. 3c,d;
447 Fig. 4b). Among the three Amundsen Sea stations, the largest movement of both Zn and Cd into
448 the particulate phase therefore occurred at station 11, concurrent with the relatively higher dFe_T
449 surface values observed at station 11 (0.2 nM dFe compared to 0.01 nM at station 4, 10 m; Fig.
450 3g, Fig. S3c). The dFe concentrations exceeding 1 nM near the seafloor are consistent with a
451 sedimentary or subglacial source (Fig. S3c). Overall, ρZn and ρCd profiles exhibited trends in
452 which values were highest within the upper 50 m at all three stations and decreased with depth,
453 following the trend in Chl a or total Chl fluorescence (Fig. 4). Vertical sections of dZn and dCd
454 through the water column mirrored these trends (Fig. 4), demonstrating the movement of these
455 dissolved metal micronutrients into the particulate phase.

456
457

Formatted: Font: Not Bold

Formatted: Font: Not Bold

Formatted: Font: Not Bold

Formatted: Font: Not Bold

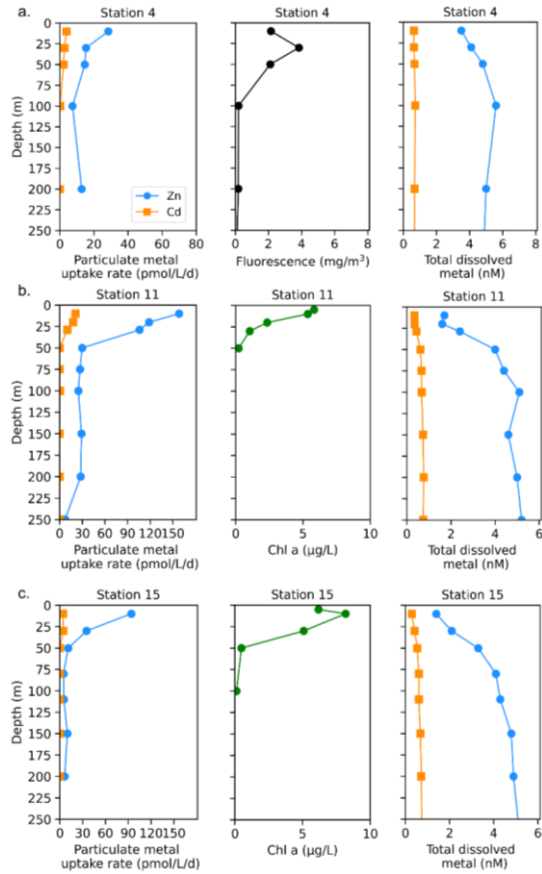
Formatted: Font: Not Bold

Formatted: Font: Not Bold

Formatted: Font: Not Bold

Formatted: Font: Not Bold

Formatted: Font: Not Bold



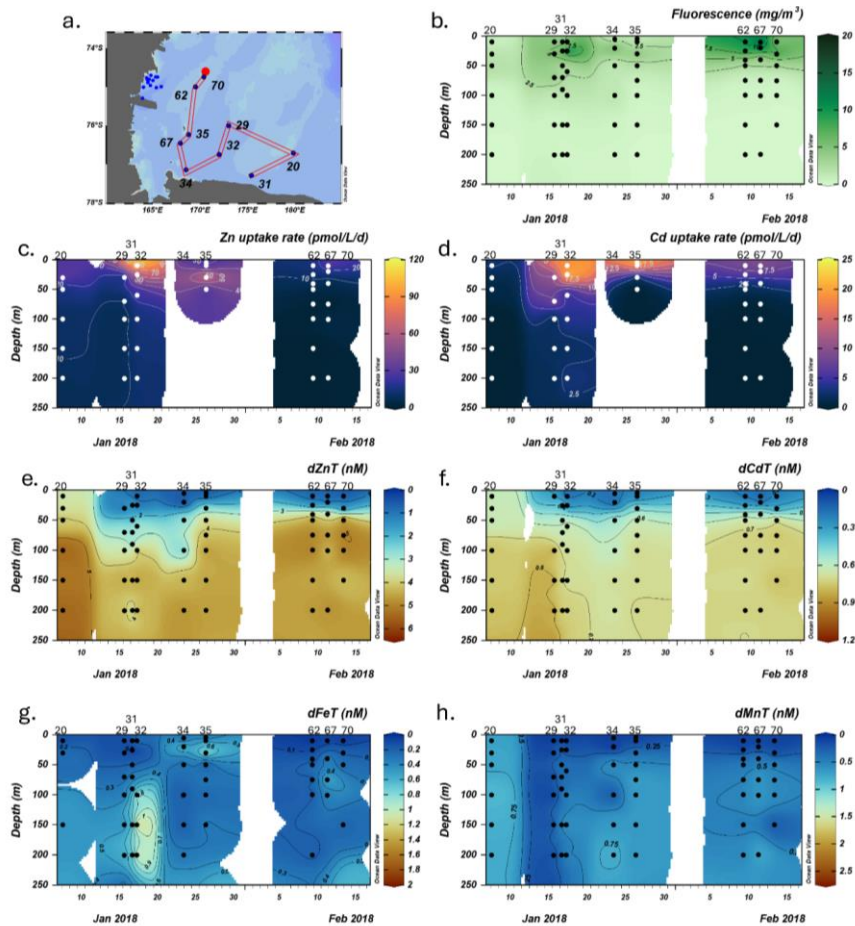
458
 459 **Figure 4.** Depth profiles of total Zn and Cd uptake rates, total chlorophyll fluorescence (or
 460 chlorophyll *a*) and total dissolved metal measured in the upper 250 m at (a) station 4, (b) station
 461 11, and (c) station 15 sampled along the Amundsen Sea shelf. Total chlorophyll (Chl)
 462 fluorescence is reported for stations where chlorophyll *a* (Chl *a*) data was not measured.
 463

464 **3.2 Ross Sea**

465 We next investigated the dissolved Zn and Cd demand of the natural phytoplankton
 466 community at stations sampled over the Ross Sea shelf. Data collected from this group is
 467 presented over time, in order of sampling date (Fig. 5).
 468

Formatted: Left

Formatted: Font: Not Bold



469

470 **Figure 5.** Total fluorescence and trace metal concentrations measured at Ross Sea stations
 471 shown over a latitudinal transect. (a) Map showing station locations, (b) total chlorophyll (Chl)
 472 fluorescence, (c) total Zn uptake rates, (d) total Cd uptake rates, (e) total dissolved Zn, (f) total
 473 dissolved Cd, (g) total dissolved Fe, and (h) total dissolved Mn measured in the upper 250 m
 474 represented in color scale. Uptake experiments were not performed at stations 31, 34, and 70.
 475 Metal concentrations measured to 800 m depth are shown in Figure S4. dZnT, total dissolved Zn;
 476 dCdT, total dissolved Cd; dFeT, total dissolved Fe; dMnT, total dissolved Mn.
 477

478 We note that unlike the Amundsen Sea sector, the stations sampled in this group did not
 479 follow a linear cruise track, thus we cannot make inferences regarding latitudinal or longitudinal

480 changes. Surface Chl fluorescence was highest at stations 32 and 67 with maximum values of
481 15.8 and 14.6 mg m⁻³ at 25 m and 10 m, respectively (Fig. 5b). With the exception of station 20,
482 dZn and dCd demonstrated high levels of surface depletion within the upper 25 m (Fig. 5e,f)
483 with average concentrations of 0.63 ± 0.13 nM and 0.19 ± 0.09 nM respectively at ≤ 10 m.
484 Compared to 100 m values (i.e., below the MLD), concentrations at 25 m were equivalent to
485 87%, 34%, 85%, 85%, 77%, and 88% decreases in dZn and 83%, 19%, 84%, 67%, 64%, and
486 75% decreases in dCd at stations 32, 20, 67, 35, 29, and 62, respectively. Measured dMn
487 concentrations were also highly depleted within the upper 250 m at all Ross Sea stations
488 (average 10 m dMn = 0.18 ± 0.26 nM; Fig. 5h). While dFe was depleted within the upper 10 m at
489 all stations (average dFe concentration at 10 m = 0.12 ± 0.12 nM), concentrations exceeding 1
490 nM were observed below 100 m at station 32 (Fig. 5g) and extended down to 650 m (Fig. S4c),
491 implying a sedimentary source. The largest Zn uptake rate measured among all stations in this
492 group (115 pmol L⁻¹ d⁻¹) was observed at station 32, 10 m (Fig. 6c). As observed in the
493 Amundsen Sea, ρZn, ρCd and total Chl a or Chl fluorescence profiles exhibited surface maxima
494 and became depleted with depth and were again mirrored by nutrient-like dZn and dCd depth
495 profiles (Fig. 6), indicative of uptake of these metals into the particulate phase in surface waters.
496

Formatted: Font: Not Bold

Formatted: Font: Not Bold

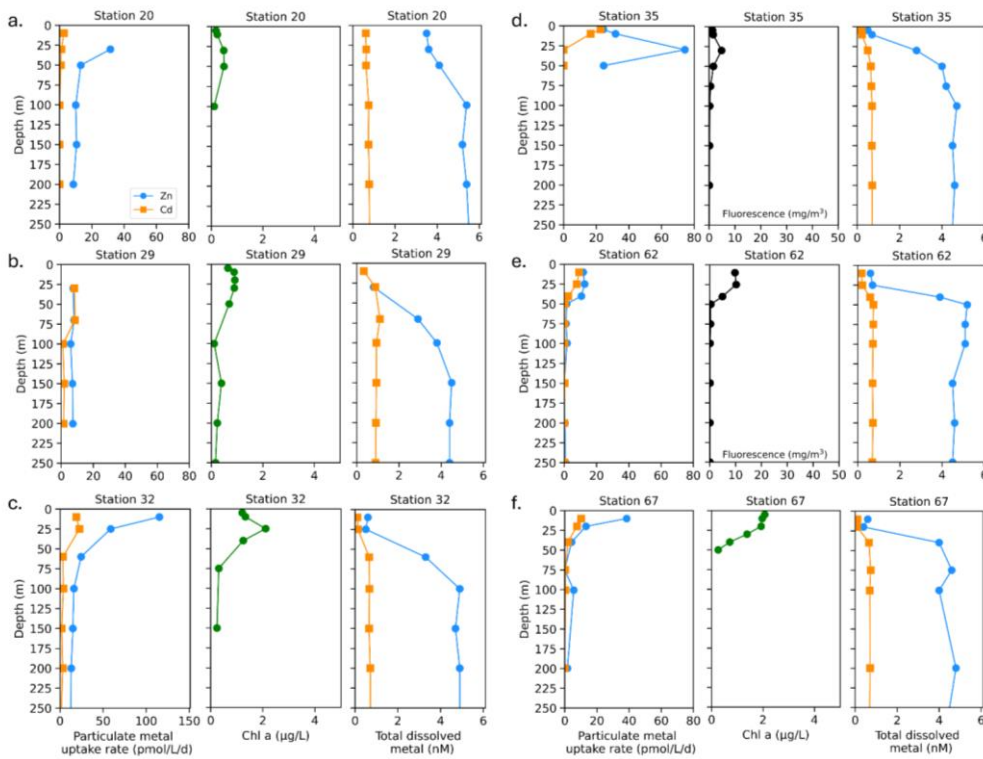
Formatted: Font: Not Bold

Formatted: Font: Not Bold

Formatted: Font: Not Bold

Formatted: Font: Not Bold

Formatted: Font: Not Bold



497

498 **Figure 6.** Depth profiles of total Zn and Cd uptake rates, total chlorophyll fluorescence (or,
 499 where available, chlorophyll a), and total dissolved metal (dMetal_T) measured in the upper 250 m
 500 at (a) station 20, (b) station 29, (c) station 32, (d) station 35, (e) station 62, and (f) station 67
 501 sampled along the Ross Sea shelf. Total chlorophyll (Chl) fluorescence is reported for stations
 502 where chlorophyll a (Chl a) data was not measured.
 503

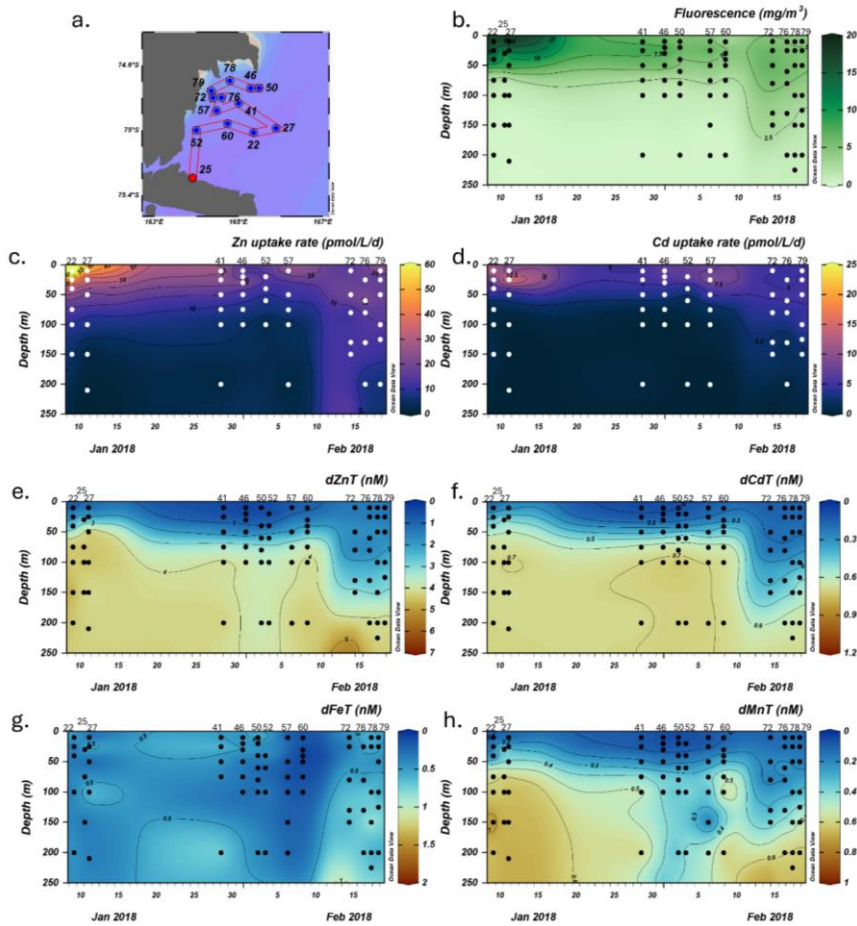
504 3.3 Terra Nova Bay

505 Zinc and Cd uptake rate data collected from stations sampled in Terra Nova Bay (TNB)
 506 were visualized over time due to repeated sampling within a small geographic region and similar
 507 timeframe (Fig. 7a). This allowed for an analysis of how dissolved metal concentrations and
 508 metal uptake rates changed throughout January-February 2018 within the same spatial area.

Formatted: Font: Not Bold

509 Station data is presented in order of sampling date, from the earliest (station 22, sampled in early
 510 January) to the latest (station 79, sampled in late February).

511



512

513 **Figure 7.** Total fluorescence and trace metal concentrations measured at Terra Nova Bay (TNB)
 514 stations shown over time. (a) Map showing station locations, (b) total chlorophyll (Chl)
 515 fluorescence, (c) total Zn uptake rates, (d) total Cd uptake rates, (e) total dissolved Zn, (f) total
 516 dissolved Cd, (g) total dissolved Fe, and (h) total dissolved Mn measured in the upper 250 m
 517 represented in color scale. Uptake experiments were not performed at stations 70 and 34. Metal
 518 concentrations measured to 600 m depth are shown in Figure S5. dZnT, total dissolved Zn;
 519 dCdT, total dissolved Cd; dFeT, total dissolved Fe; dMnT, total dissolved Mn.

520

521 Surface Chl fluorescence was highest in early January ($\sim 18 \text{ mg m}^{-3}$) and waned into
522 February (Fig. 7b), similar to observed trends in Zn and Cd uptake rates (Fig. 7 c,d). Of all TNB
523 stations, stations 22 and 27, sampled in January, had the highest maximum Zn uptake rates of
524 $89.9 \text{ pmol L}^{-1} \text{ d}^{-1}$ and $46.0 \text{ pmol L}^{-1} \text{ d}^{-1}$, respectively, at 10 m (Fig. 8a,b). Cd uptake rates were
525 also highest at these stations with values of $13.4 \text{ pmol L}^{-1} \text{ d}^{-1}$ and $20.1 \text{ pmol L}^{-1} \text{ d}^{-1}$ (Fig. 8a,b). At
526 the final station (station 79, sampled in late February) maximum uptake rates of both metals had
527 sharply decreased to $24.7 \text{ pmol Zn L}^{-1} \text{ d}^{-1}$ and $5.0 \text{ pmol Cd L}^{-1} \text{ d}^{-1}$ (Fig. 8i). Overall, maximum
528 uptake rates of both metals decreased over time within TNB (Fig. 7c,d), consistent with the
529 decrease in total Chl fluorescence (Fig. 7b) likely due to the aging and decline of the
530 phytoplankton bloom.

531 Surface depletion of dZn, dCd, and dMn was observed at all stations with average
532 dissolved concentrations of $0.82 \pm 0.47 \text{ nM Zn}$, $0.13 \pm 0.06 \text{ nM Cd}$, and $0.08 \pm 0.04 \text{ nM Mn}$ at
533 10 m depth (Fig. 7e,f,h). Notably, increased surface concentrations of dZn, dCd, and dMn were
534 apparent at the late stations 72, 76, 78 and 79, with dZn $\sim 2 \text{ nM}$, dCd $\sim 300 \text{ pM}$, and dMn ~ 0.2
535 nM (Fig. 7e,f,h; Fig. S5). Dissolved macronutrient (phosphate, nitrate and nitrite, and silicate)
536 concentrations also followed this trend, with increased surface concentrations at the late stations
537 (Fig. S6). As with the Amundsen and Ross Sea station groups, Zn and Cd uptake rates within
538 TNB tended to be highest at the surface $\leq 50 \text{ m}$ as also observed in total Chl fluorescence trends
539 and mirrored the decrease in total dissolved Zn and Cd (Fig. 8). Unlike the Amundsen and Ross
540 Sea stations, where Cd uptake consistently became negligible ($\sim 0 \text{ pM L}^{-1} \text{ d}^{-1}$) by 100 m (Fig. 4;
541 Fig. 6), measurable Cd uptake persisted in TNB to 150 m at stations 72 and 79 (Fig. 8g,i).
542 Measurable Zn uptake rates were also captured at deeper depths at these late TNB stations (Fig.
543 8g,h,i).

Formatted: Font: Not Bold

Formatted: Font: Not Bold

Formatted: Font: Not Bold

Formatted: Font: Not Bold

Formatted: Font: Not Bold

Formatted: Font: Not Bold

Formatted: Font: Not Bold

Formatted: Font: Not Bold

Formatted: Font: Not Bold

Formatted: Font: Not Bold

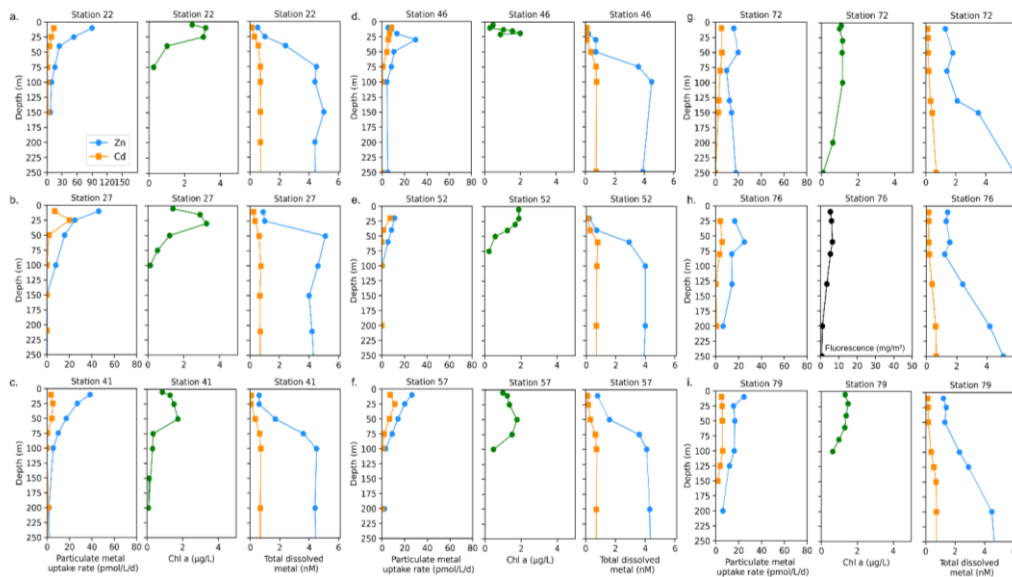
Formatted: Font: Not Bold

Formatted: Font: Not Bold

Formatted: Font: Not Bold

Formatted: Font: Not Bold

Formatted: Font: Not Bold



544

545 **Figure 8.** Depth profiles of total Zn and Cd uptake rates, total chlorophyll fluorescence (or,
 546 where available, chlorophyll a), and total dissolved metal (dMetalT) measured in the upper 250
 547 m at (a) station 22, (b) station 27, (c) station 41, (d) station 45, (e) station 52, (f) station 57, (g)
 548 station 72, (h) station 76, and (i) station 79 within Terra Nova Bay. Total chlorophyll (Chl)
 549 fluorescence is reported for stations where chlorophyll a (Chl a) data was not measured.
 550

551 The increased surface concentrations of dZn and dCd and macronutrients, as well as the
 552 persistence of measurable uptake rates at deeper depths, at these late TNB stations may be

553 attributed to the deepening of the mixed layer (Fig. S7). Vertical mixing was evidenced by more

554 uniform potential densities, temperatures, dissolved oxygen (O₂) concentrations, salinity, and

555 beam transmission measurements at the late TNB stations within the upper 200 m (Fig. S7).

556 Higher (>0.5 nM) dFe concentrations were also observed below 100 m at these late stations (Fig.

557 7g) and increased with depth (>2 nM), as did dZn and dMn concentrations, possibly due to

558 sedimentary inputs (Giordano et al., 1999) (Fig. S5). At these late stations (Station 76, 78, 79)

559 mixing replenished surface concentrations of both macronutrients (Fig. S6) and dZn (Fig. S5a),

Formatted: Font: Not Bold

Formatted: Font: Not Bold

Formatted: Font: Not Bold

Formatted: Font: Not Bold

Formatted: Font: Not Bold

Formatted: Font: Not Bold

560 but dZn was replenished to a lower extent. For example, comparing 50 m “replenished” surface
 561 values of P, N+N, and Si to deepwater (200 m) values at Station 79, percent changes from deep
 562 to surface values were -0.35% for P, -0.30% for N+N, and -0.26% for Si (where a percent%
 563 change of 0 would indicate complete replenishment; i.e, if nutrient values at 200 m and at 50 m
 564 were equal). In contrast, the percent change from deep (200m) to surface (50m) dZn at Stn79
 565 was lower, -0.71%. Hence, dZn was apparently replenished to a lesser extent compared to
 566 macronutrients, which may reflect a sustained high demand for Zn generating a dearth of this
 567 micronutrient despite macronutrient replenishment.

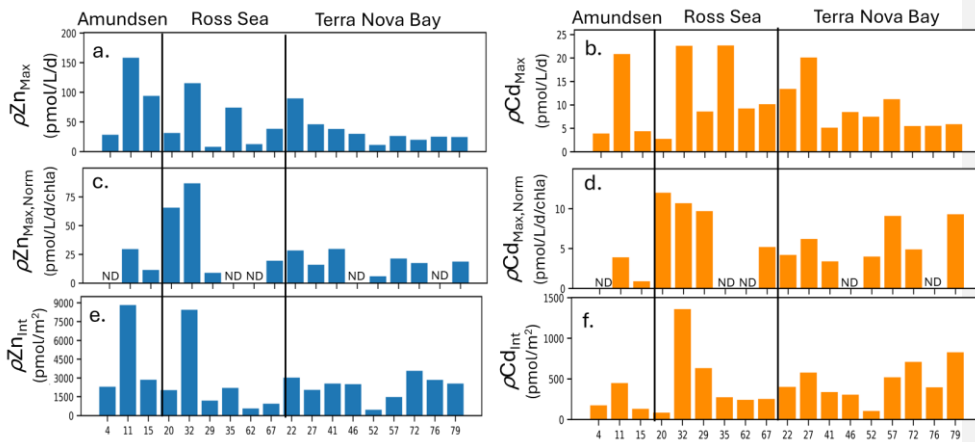
568 **4 Discussion**

569 **3.44.1 Overview of Zn and Cd uptake at 18 stations**

570 We next summarize mMaximum Zn and Cd uptake rates observed at each station (all of
 571 which were observed at ≤ 10 m depth; Fig. 9a,b) with uptake rates normalized to Chl a ($\mu\text{g/L}$) as
 572 a proxy for biomass (Fig. 9c,d).

Formatted: Font: Not Bold

Formatted: Font: Not Bold



573
 574 **Figure 9.** Unnormalized (a) maximum Zn uptake rates ($\rho\text{Zn}_{\text{Max}}$) and (b) maximum Cd uptake
 575 rates ($\rho\text{Cd}_{\text{Max}}$) at each station grouped by area (Amundsen Sea, Ross Sea, Terra Nova Bay). (c)
 576 $\rho\text{Zn}_{\text{Max}}$ and (d) $\rho\text{Cd}_{\text{Max}}$ normalized to chlorophyll a ($\mu\text{g L}^{-1}$) measured at each station. (e) Depth

577 integrated (10 m-250 m) ρZn and ρCd values at each station. ND, no data (chlorophyll a not
578 measured).

579

580 Overall, high ($>25 \text{ pmol L}^{-1} \text{ d}^{-1} \text{ Chl a (ug/L)}^{-1}$) Chl a-normalized Zn uptake rates were measured

581 at station 11 in the Amundsen Sea and at stations 20 and 32 in the Ross Sea (Fig. 9c). The

Formatted: Font: Not Bold

582 highest Chl a-normalized Cd uptake rates among all 18 stations were also measured at stations

583 20 and 32 (Fig. 9d). Across TNB, Chl a-normalized maximum Zn and Cd uptake ranged from

Formatted: Font: Not Bold

584 $6.0 - 28.3 \text{ pmol L}^{-1} \text{ d}^{-1} \text{ Chl a}^{-1}$ for Zn, and $3.4 - 9.3 \text{ pmol L}^{-1} \text{ d}^{-1} \text{ Chl a}^{-1}$ for Cd; Fig. 9c,d).

Formatted: Font: Not Bold

585 Integrated (10 m-250 m) uptake rate values were highest for Zn at stations 11 and 32, and highest

586 for Cd at station 32 (Fig. 9e,f). Increases in integrated Cd and Zn uptake at the late stations 72,

Formatted: Font: Not Bold

587 76 and 79 reflected the deeper depths to which uptake rates of these metals remained measurable,

588 likely reflecting deepened mixed layers (Fig. S7) and/or sinking of the phytoplankton

Formatted: Font: Not Bold

589 community, as seen in the fluorescence data to beyond 150m depth (Fig. 7b). The presence of

Formatted: Font: Not Bold

590 Chl a (Fig. 8g,i) implies these deep phytoplankton communities may ~~have been still be~~ alive, if

Formatted: Font: Not Bold

591 not actively photosynthesizing. We previously identified ZCRP-B, a membrane-associated

592 protein involved in high-affinity Zn transport (Kellogg et al., 2022). These proteins have a single

593 transmembrane domain, implying function as a membrane-tethered ligand to assist in the

594 acquisition of Zn from seawater in cooperation with adjacent zinc transporters (ZIP transporters).

595 Hence ZCRP-B could be a potential site of Zn binding and ‘uptake’, as our uptake rate

596 measurements do not discern between extracellular and intracellular Zn, even if the

597 phytoplankton are inactive due to a lack of photosynthetic energy at these depths.

598 Notably, maximum Cd uptake rates measured in the present study were 3.4, 3.7, and 3.3

Formatted: Indent: First line: 0.5"

599 times higher in the Amundsen Sea, Ross Sea, and Terra Nova Bay, respectively, compared to the

600 maximum Cd uptake rate of $6.1 \text{ pmol L}^{-1} \text{ d}^{-1}$ measured previously within the Costa Rica Dome

601 [using identical methods \(Cox et al., 2014\), demonstrating the influence of high productivity and](#)
602 [the native community on the flux of dCd into the particulate phase.](#)

603 **4 Discussion**

604 **4.12 Use of metal uptake rates to determine depletion timeframes**

605 The measurement of total dissolved metal concentrations over large latitudinal or
606 longitudinal areas allows for the characterization of metal inventories, though these are snapshots
607 of inventories observed at specific times. The measurement of metal uptake rates allows us to
608 gain new insight into how these inventories came to be and the timeframes over which they are
609 consumed and replenished. Due to the resetting of surface dissolved metal concentrations to
610 those of deepwater values during austral winter with deep winter mixing, the Ross Sea of the
611 Southern Ocean is particularly applicable to this type of timeframe study (Sedwick and DiTullio
612 1997; Sedwick et al. 2011).

613 Using the Zn uptake rates measured in this study, we can estimate the time required for
614 the high levels of primary production observed in the Southern Ocean to draw down surface dZn
615 from high (deep water) winter concentrations to the surface concentrations observed during
616 austral summer 2017. The Southern Ocean growing season typically spans October-March, with
617 primary productivity peaking November-January and the area of open (ice-free) water over the
618 Ross Sea shelf linearly increasing from November-mid January (Sedwick et al., 2011). Vertical
619 profiles of nutrients and micronutrients in coastal Antarctic ecosystems such as the Ross Sea are
620 reset and become uniform with depth during the winter months due to whole-water column
621 mixing and an absence of photosynthetic activity during the dark winter under the sea ice (Noble
622 et al., 2013). As a result, the drawdown of nutrients in the upper water column observed during
623 the spring and summer seasons is the result of less than one year's biological influence. For this

624 simple calculation, we ignore the upward flux of Zn (upwelling = 0) and assume a high export
 625 ratio of 0.8 due to bloom productivity being dominated by diatoms and *Phaeocystis antarctica*,
 626 both of which sink rapidly and thus contribute substantially to carbon export flux (Asper and
 627 Smith 1999; DiTullio et al. 2000). The depletion of dZn from a surface box was therefore
 628 estimated as:

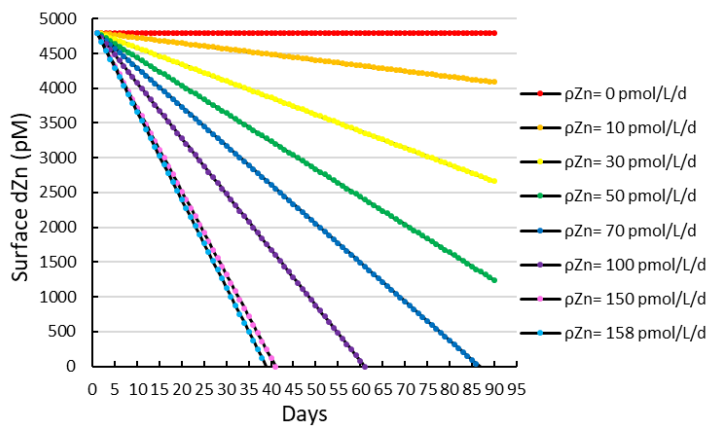
629
$$\left(\frac{dZn}{dt}\right)_{\text{surface box}} = -\rho Zn + (Rf * \rho Zn) + \text{upwelling}$$

630 Where Rf is the remineralization factor equal to 1 - export ratio.

631 Taking station 11, for which the highest Zn uptake rate was observed, as an extreme case:
 632 with a maximum Zn uptake rate of 158 pmol L⁻¹ d⁻¹, it would take only 25 days to deplete a
 633 surface winter concentration of 4.8 nM (that is, the ambient average deepwater (< 200 m) dZn
 634 concentration for all stations measured in this study: Fig. 4b) down to the observed ambient
 635 surface concentration of 1.7 nM at station 11 (Fig. 4b), assuming a constant uptake rate and no
 636 additional inputs of dissolved Zn (Fig. 10).

Formatted: Font: Not Bold

637



638

639 **Figure 10.** A simple model estimating the time (in days) required to deplete the estimated
 640 average winter surface concentration of dZn (4.8 nM) over a range of various Zn uptake rates

641 (ρ_{ZnUR}). 158 pmol/L/d was the maximum Zn uptake rate observed in this study (station 11, 10
642 m).
643

644 Given that dZn surface depletion to sub-nanomolar levels was observed throughout much
645 of the CICLOPS expedition, prolonged high levels of Zn uptake and export that overwhelm
646 replenishment by vertical mixing and/or remineralization are likely key to giving rise to the
647 observed extent of seasonal surface dZn depletion. These calculations were conducted as a proof-
648 of-concept to determine if uptake rates were sufficient to draw down the otherwise abundant dZn
649 inventory on seasonal timescales. An important caveat to this calculation is that the regulation
650 and production of Zn sensors that modulate Zn uptake, export, and storage will naturally
651 fluctuate in response to changing dZn and therefore cannot be assumed as a constant. Future
652 studies could conduct mesoscale modeling of the region, ~~replacing upwelling~~-including eddy
653 diffusion and advection. Notably, any dZn upwelling flux into the euphotic zone would require
654 even higher Zn uptake rates to create the seasonal surface Zn depletion we observed on this
655 expedition.

656

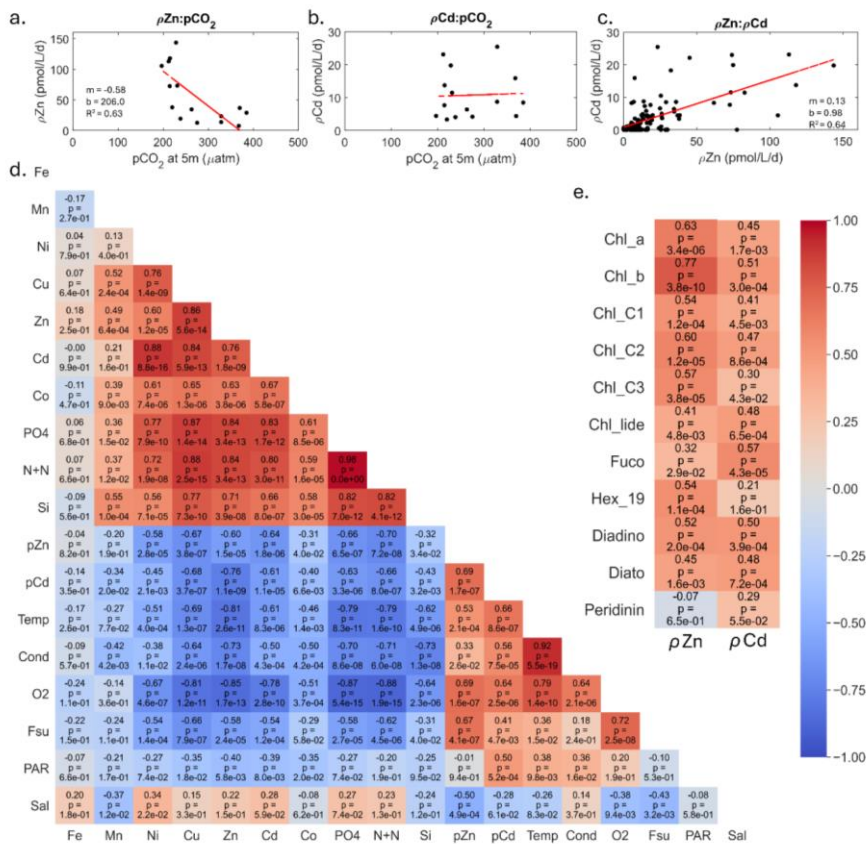
657 **4.2.3 Influences on Zn and Cd uptake**

658 We next consider the factors driving the magnitude of ρ_{Zn} and ρ_{Cd} . As noted above, ρ_{Zn}
659 and ρ_{Cd} were positively correlated with total Chl fluorescence or Chl *a* at every station (Fig. 4;
660 Fig. 6; Fig. 8), demonstrating the influence of total autotrophic biomass on uptake rates. A
661 Pearson correlation analysis comparing the abundance of individual algal pigments to ρ_{Zn} and
662 ρ_{Cd} throughout the water column for all stations revealed significant, positive correlations
663 (Pearson correlation coefficient > 0.50 , $p \leq 1.2e-4$) between ρ_{Zn} and Chl *a*, Chl *b*, and Chl *c*1, *c*2
664 and *c*3. Pearson correlation coefficients are normally symbolized as rho (ρ), but to avoid

Formatted: Font: Not Bold

665 confusion with our uptake rate symbol (ρ), and with p-values (p), they are herein referred to as
 666 'PCC_{ee}' values. The correlation between ρ Zn and Chl *b* was strongest (PCC_{ee}= 0.77, p = 3.8e-
 667 10) of any pigment (Fig. 11e).

Formatted: Font: Not Bold



668
 669 **Figure 11.** Relationships comparing seawater CO₂ partial pressure (pCO_2) at 5 m depth to (a) Zn
 670 uptake rates (ρ Zn; n=15, $R^2 = 0.63$) and (b) Cd uptake rates (ρ Cd; n=15) measured at surface
 671 (≤ 10 m) depths. (c) Relationship between ρ Zn and ρ Cd for all depths (n=121, $R^2 = 0.64$). (d)
 672 Visual representation of the correlation matrix comparing all water column parameters measured
 673 with depth with warm and cool colors indicative of positive and inverse correlations,
 674 respectively. Pearson correlation coefficients and p values are shown. (e) Representation of the
 675 correlation matrix comparing ρ Zn and ρ Cd to various phytoplankton pigments. Fe, Mn, Ni, Cu,
 676 Zn, Cd, and Co labels correspond to total dissolved metal concentrations. PO₄, N+N, and Si
 677 correspond to total dissolved concentrations of phosphate, the sum of nitrate+nitrite, and silicate.

678 Temp, temperature; cond, conductivity; O₂, dissolved oxygen; Fsu, total fluorescence; PAR,
679 photosynthetically active radiation; Sal, salinity. Chl_a, chlorophyll a; Chl_b, chlorophyll b;
680 Chl_c1, chlorophyll c1; Chl_c2, chlorophyll c2; Chl_c3, chlorophyll c3; chl_lide, chlorophyllide;
681 Fuco, fucoxanthin; Hex_19, 19'-hexanoyloxyfucoxanthin; Diadino, diadinoxanthin; Diato,
682 diatoxanthin.
683

684 In bottle incubation experiments conducted at station 27, the addition of Zn alone resulted
685 in the positive growth response of Chl *b*-containing algae (small green algae such as
686 prasinophytes; (Kell et al., 2023)), corroborating this finding. ρ Cd also positively correlated with
687 these Chl pigments but with slightly lower correlation Pearson correlation coefficients ($PCC_{ee} =$
688 $0.3-0.51$; $p \leq .043$). Fucoxanthin (fuco) concentrations were more highly correlated with ρ Cd
689 ($PCC_{ee} = 0.57$, $p = 4.3e-5$) than with ρ Zn ($PCC_{ee} = 0.32$, $p = 2.9e-2$), while the opposite was
690 observed for 19'-Hex (19'-hexanoyloxyfucoxanthin; $PCC_{ee} = 0.54$, $p = 1.1e-4$ for Zn; not
691 significant for Cd) (Fig. 11e). Fuco and 19'-Hex are used as taxonomic indicators of diatoms and
692 *Phaeocystis*, respectively, in the Ross Sea (DiTullio et al., 2003, 2007; DiTullio and Smith,
693 1995; Wright et al., 2010). The higher correlation coefficient between ρ Zn and *Phaeocystis*
694 abundance (as indicated by 19'-Hex) implies that Zn uptake was driven largely by *Phaeocystis*.
695 This finding is consistent with the detection of *Phaeocystis* ZCRP-A, a protein characterized as
696 an algal Zn²⁺ metallochaperone (Kellogg et al., 2022), in metaproteomic data collected from both
697 the incubation experiment and throughout the water column at station 27 (Kell et al., 2023). The
698 positive correlation between ρ Cd and the abundance of diatoms (as indicated by fuco) is
699 consistent with the diatomic utilization of Cd as a nutrient within CDCA metalloenzymes, as
700 *cdca* genes have, to date, been found exclusively in diatom species (Park et al., 2007, 2008).
701 While it is likely that both *Phaeocystis* and diatoms contributed to the Cd and Zn uptake rates
702 measured here, it is currently unknown if *Phaeocystis* can utilize Cd as a nutrient. Overall, any
703 potential growth benefit conferred by our Cd spike additions may only have been applicable to

Formatted: Font: Not Bold

704 diatoms that 1) possessed the *cdca* gene and 2) faced selection pressure to utilize Cd as a
705 cofactor in CDCA due to low seawater pCO₂ (as documented on this expedition) creating
706 enhanced demand for dZn. The presence of Cd-utilizing diatoms in the water column at station
707 27 was demonstrated by the detection of CDCA transcripts with closest taxonomic matches to
708 the diatom genera *Chaetoceros* and *Corethron* (Kell et al., 2023). Station 27 also exhibited high
709 surface Chl fluorescence (19.3 mg m⁻³ at 10 m), low pCO₂ (221 μatm at 5 m), and high
710 maximum Zn and Cd uptake rates (46 and 20 pmol L⁻¹ d⁻¹, respectively), demonstrating a high
711 algal demand for Zn that likely created pressure for Cd uptake.

712 We next consider the effect of the depleted seawater pCO₂ levels induced by the high
713 biomass conditions observed on this expedition. Previously, a strong correlation between
714 dissolved δ¹¹⁴Cd and dissolved CO₂ was documented in the Atlantic Sector of the Southern
715 Ocean (de Baar et al., 2017), suggesting significant Cd isotope fractionation due to biological
716 uptake into the particulate phase. A relationship between total surface Cd uptake rates at 10 m
717 and surface pCO₂ (underway, measured at 5 m) was not observed in the present study (Fig. 11b).
718 The present study includes measurements of total Cd uptake (that is, the sum of all Cd isotopes)
719 using an added Cd isotope tracer, and hence did not explore natural isotope fractionation effects.
720 However, we did observe a significant negative linear relationship between total Zn uptake rates
721 and seawater pCO₂ ($m = -0.58$; $R^2 = 0.63$; Fig. 11a) consistent with an increased demand for Zn²⁺
722 to power the carbon concentrating mechanism of photosynthetic algae under lower CO₂
723 availability. ρ_{Zn} and ρ_{Cd} furthermore shared a significant positive linear relationship with each
724 other ($m = 0.13$; $R^2 = 0.64$; Fig. 11c) (as was also reflected in the Pearson correlation test; PCC =
725 0.69, $p = 1.7e-7$, Fig. 11d) implying that as demand for Zn increased, demand for Cd also
726 increased, consistent with laboratory studies showing their co-transport in marine algae (Sunda

Formatted: Font: Not Bold

Formatted: Font: Not Bold

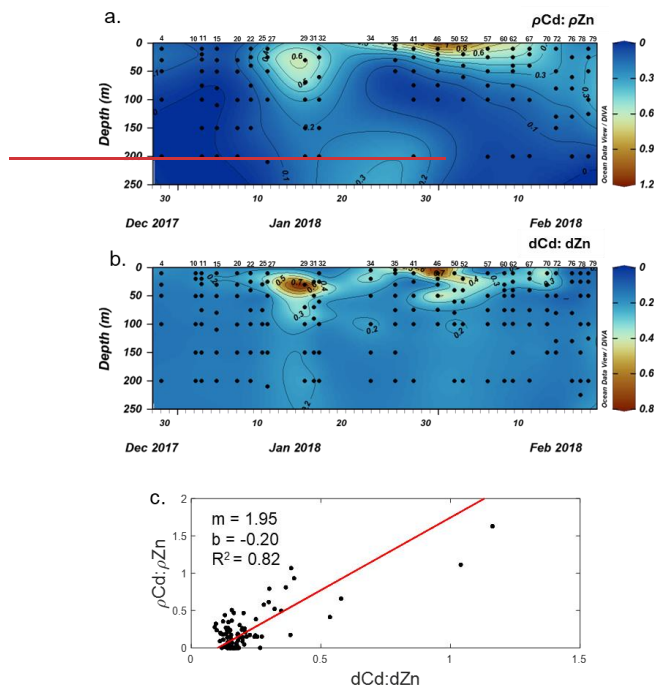
Formatted: Font: Not Bold

Formatted: Font: Not Bold

727 and Huntsman, 2000). We also note that $\rho\text{Cd}:\rho\text{Zn}$ uptake ratios were higher (> 0.4) at the surface
728 where total dissolved $\text{dCd}:\text{dZn}$ ratios were comparatively higher (> 0.3) (Fig. S812a,b). The
729 strong positive linear relationship shared between these ratios ($R^2 = 0.82$; Fig. S812c) further
730 suggests that dZn levels were depleted enough to induce increased Cd uptake rates, and is
731 consistent with their known biochemical substitution within marine algae.

Formatted: Font: Not Bold

Formatted: Font: Not Bold



732
733 **Figure 12.** (a) Cd:Zn uptake ratios ($\rho\text{Cd}:\rho\text{Zn}$) and (b) total dissolved Cd:Zn ratios ($\text{dCd}:\text{dZn}$) for
734 all stations during the CICALOPS expedition measured in the upper 250 m represented in color
735 scale and over time of sampling. (c) Two-way linear regression showing the positive relationship
736 between $\text{dCd}:\text{dZn}$ and $\rho\text{Cd}:\rho\text{Zn}$ inclusive of all stations and depth ($n=111$, $R^2=0.82$).
737

738 Algal Cd uptake rates are known to be inversely related to both Mn^{2+} and Zn^{2+}
739 concentrations in culture (Lee et al., 1995; Sunda and Huntsman, 1996), which is thought to
740 reflect the uptake of Cd by two separate inducible transport systems. Cadmium-Cd is taken up

741 competitively by the high-affinity Zn uptake system under low Zn^{2+} conditions, as demonstrated
742 above, while Cd, Zn, and Mn share the same low-affinity Mn uptake system under high Zn^{2+}
743 conditions (Lee et al., 1995; Sunda and Huntsman, 1998b, a, 2000; Xu et al., 2007). With the
744 exception of the Amundsen Sea stations, dMn was consistently observed at concentrations of
745 only 0.1-0.5 nM within the upper 50 m (Fig. 3h; Fig. 5h; Fig. 7h). Low surface dMn
746 concentrations within the Southern Ocean have been documented previously and were attributed
747 to a combination of biological uptake at the surface causing depletion and low resupply due to
748 few external sources (Latour et al., 2021). While ρCd was negatively correlated with dMn (PCC
749 = -0.34, $p = 0.02$) considering all stations and all depths, ρCd was more strongly negatively
750 correlated with dZn (PCC = -0.76, $p = 1.1e-9$), which was the strongest negative correlation
751 comparing all measured parameters to ρCd (Fig. 11d). This finding is consistent with decreased
752 dCd uptake where dZn availability is sufficient. Overall, these results are consistent with biology
753 (total biomass) and pCO_2 acting as primary influences on ρZn , with increases in ρZn leading to
754 increases in ρCd through the upregulation of a shared transport system.

Formatted: Font: Not Bold

Formatted: Font: Not Bold

755 **4.3 Effects on dCo cycling**

Formatted: Font: Bold

756 In addition to Cd, the intense Zn demand captured by these uptake rates also appears to
757 have shifted the demand for the trace metal micronutrient cobalt (Co) (Chmiel et al., 2023). Due
758 to their similar charge and atomic radii, Zn^{2+} , Co^{2+} and Cd^{2+} cations often share the same
759 transporter uptake systems. An organism's ability to utilize these metals as metabolic cofactors is
760 influenced by their environment and the affinity of the uptake ligands for each metal cation
761 (Irving and Williams, 1953; Sunda and Huntsman, 1992). When dZn availability is low, more
762 dCd and dCo are able to bind transport ligands. Therefore, dZn concentrations and cycling can
763 influence the cycling of dCd and dCo, particularly in low dZn environments as documented for

Formatted: Indent: First line: 0.5"

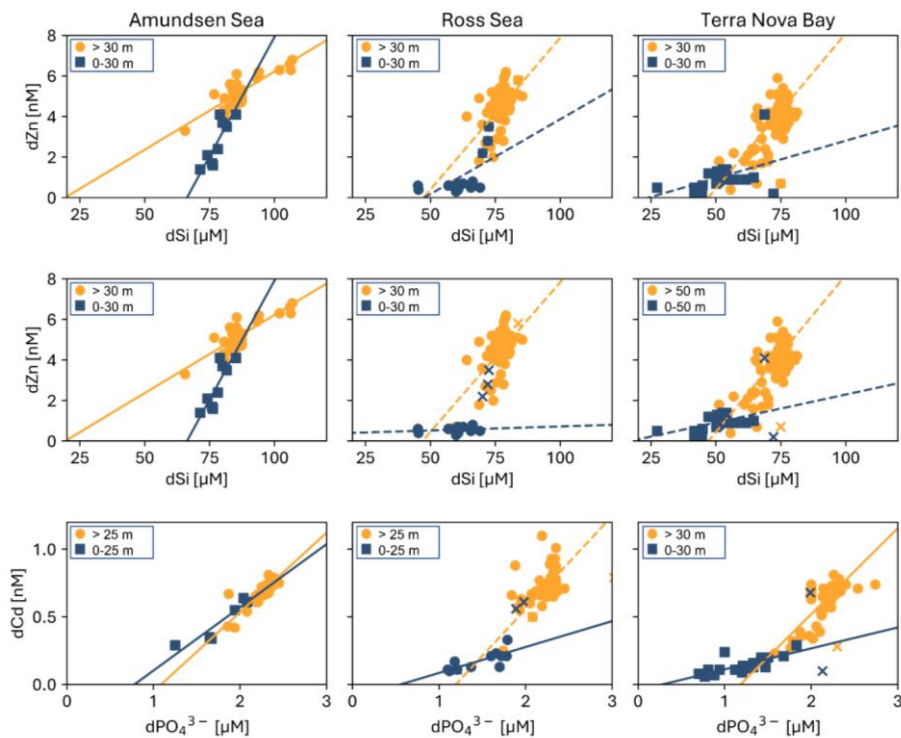
764 dCd in the present study. The influence of dZn cycling on dCo distributions in this region was
765 also documented during this expedition, with evidence for high rates of biological Co uptake in
766 the Ross Sea driven by dZn (and vitamin B₁₂) scarcity (Chmiel et al., 2023). The high Zn uptake
767 rates measured in this study therefore also reveal dynamic changes in the cycling of Cd and Co
768 as a consequence of high Zn demand.
769

770 **4.4 dZn and dCd relationships with macronutrients**

771 The growth of phytoplankton and bacteria in the shallow euphotic zone results in the
772 removal of bioactive trace metals and macronutrients from the dissolved phase into the
773 particulate phase, resulting in dissolved metal:macronutrient relationships that reflect their
774 collective stoichiometry (Horner et al., 2021). Positive linear slopes result generally indicate the
775 co-cycling of the metal and the macronutrient via uptake and remineralization, though slope
776 values can vary widely by basin as they are a function of the metal:macronutrient uptake and
777 remineralization stoichiometry of the native community and overall nutrient availability. Two-
778 way linear regressions (see Methods) were used to investigate the relationships between dZn and
779 dissolved silicate (dSi), dZn and dissolved phosphate (dP), and dCd and dP for the Amundsen
780 Sea, Ross Sea, and TNB station groups (Fig. 123).

Formatted: Font: Not Bold

Formatted: Font: Not Bold



784
 785 **Figure 123.** Relationships between (Top row) total dissolved Zn and silicate (dSi), (Middle row)
 786 total dissolved Zn and phosphate (dPO_4^{3-}), and (Bottom row) total dissolved Cd and dPO_4^{3-} for
 787 surface (blue squares) and deep ocean (orange circles) arranged by station group (Amundsen
 788 Sea, Ross Sea, and Terra Nova Bay). Depth thresholds were manually chosen to optimize the
 789 linear fit of the surface and deep ocean trends. Regressions with an $R^2 \geq 0.50$ are shown as a
 790 solid line, and those with an $R^2 < 0.50$ are shown as a dotted line. See Table S4 for
 791 stoichiometric parameters and values. Regression outliers are marked with an 'x'. Data originally
 792 plotted in Chmiel et al. 2023 and reprised here for ease of comparison with dZn:Si data.
 793

Formatted: Font: Not Bold

794 The dZn:dP and dCd:dP relationships from this expedition were originally presented in
 795 Chmiel et al. 2023 for comparison to dCo:dP, while they are included in the present study for
 796 ease of comparison with dZn:dSi relationships presented for the first time. For these analyses, the
 797 depth threshold that separates the surface and deep ocean was manually defined in order to
 798 optimize the linear fit of the surface versus deep trends— this threshold depth can be thought of

799 as an inflection point that represents the largest change in trace metal concentration with respect
800 to dP or dSi concentration (Chmiel et al., 2023).

801 ~~As noted above,~~ the near-linear global dZn:dSi relationship (Bruland et al., 1978;
802 Middag et al., 2019; Vance et al., 2017) has been posited to arise, in part, from faster drawdown
803 of Zn and Si relative to dPO_4^{3-} into Southern Ocean diatoms that leaves surface waters Zn and Si
804 depleted (Vance et al., 2017). We observed distinct differences in dissolved dZn:dSi ecological
805 stoichiometries comparing Amundsen Sea, Ross Sea and Terra Nova Bay station groups (Fig.
806 123; Table S4). A positive linear dZn:dSi relationship with a steep ($m = 0.23 \pm 0.05$; Table S4)
807 slope observed in the upper ocean of the Amundsen Sea contrasted starkly with the shallow
808 slopes observed in the upper ocean of the Ross Sea and Terra Nova Bay. A bloom of non-
809 silicifying *Phaeocystis antarctica* was present during our passage through the Amundsen Sea,
810 consistent with abundant silicic acid yet rapid draw-down of Zn, which is known to be used by
811 this organism (Saito and Goepfert, 2008). In contrast, the shallow slopes in the Ross Sea and
812 Terra Nova Bay resulted from the persistence of dSi concentrations $\geq 30 \mu\text{M}$ in the upper 30 m,
813 while dZn was reduced to sub-nanomolar concentrations (average dZn = $0.87 \pm 0.42 \text{ nM}$ in TNB
814 at 10 m depth, $n = 11$), highlighting the intense drawdown of dZn by biota in this region to meet a
815 high metabolic dZn demand.

816 Similar trends were observed for dZn:dP and dCd:P, which exhibited shallow slopes
817 within the upper ocean of the Ross Sea and Terra Nova Bay. Southern Ocean diatoms are known
818 to have Zn:P uptake ratios that are up to an order of magnitude greater than the average for
819 oceanic phytoplankton (Sieber et al., 2020; Twining and Baines, 2013; Vance et al., 2017). The
820 increased presence of diatoms (as indicated by higher fucoxanthin concentrations) at the late
821 stations within Terra Nova Bay therefore likely exacerbated the surface decoupling of dZn and

Formatted: Font: Not Bold

Formatted: Font: Not Bold

822 dP due to their high dZn demand. The maximum uptake rates of 158, 115, and 89 pmol Zn L⁻¹ d⁻¹
823 measured in this study for the Amundsen Sea, Ross Sea, and Terra Nova Bay groups,
824 respectively, contextualize the high Zn uptake rates hypothesized to contribute to the high dZn:
825 dP uptake ratios observed in Southern Ocean diatoms. These rates are indicative of total potential
826 biological uptake, likely influenced by a depleted labile Zn pool and residual of complexed Zn,
827 that then results in low dZn:dP ratios in shallow waters.

828 Like dZn and dSi, dCd and dP concentrations are known to share strong correlations in
829 both deep and surface seawater (de Baar et al., 1994; Boyle, 1988; Boyle et al., 1976), with the
830 vertical distribution of Cd controlled by phytoplankton uptake in surface waters and sinking of
831 particulate organic matter and subsequent remineralization at depth. Observations of enhanced
832 Cd uptake within the Fe-limited Southern Ocean (Cullen, 2006) are consistent with observations
833 of increased Cd uptake by marine algal species under Fe limitation in both the field (Baars et al.,
834 2014; Cullen et al., 2003; Cullen and Sherrell, 2005) and in culture (Lane et al., 2009; Sunda and
835 Huntsman, 2000), thought to be due to the increased use of Cd in biochemical processes or
836 inadvertent uptake due to the upregulation of metal transporters (Cullen, 2006; Sunda and
837 Huntsman, 2000). In these coastal regions, dCd:dP had the same regional and depth trends as
838 dZn:dP, further demonstrating their close biogeochemical association.

839 **5 Conclusions**

840 We have quantified the movement of the trace metals Zn and Cd from the dissolved to
841 the particulate phase within the phytoplankton >3 μm size fraction collected in the Amundsen
842 Sea, Ross Sea, and Terra Nova Bay of the Southern Ocean during austral summer 2017-2018.

843 ~~Increases in particulate ¹¹⁰Cd and ⁶⁷Zn concentrations in spiked samples, increases in particulate~~
844 ~~⁶⁷Zn: ⁶⁸Zn and ¹¹⁰Cd: ¹¹⁴Cd sample ratios relative to controls, and surface depletion of total~~

845 dissolved Zn and Cd concentrations apparent at all 18 stations demonstrated metal uptake into
846 the particulate phase mainly within the upper 50 m. Our study confirms the utility of the adapts
847 the stable 24hr Cd-stable isotope tracer uptake method employed (Cox et al., 2014), and expands
848 its use to the measurements of Zn uptake, and represents the first Zn time series measurements of
849 dZn and Zn uptake in a coastal environment during a bloom event. We have found that these
850 high observed uptake rates were sufficient to draw down the otherwise abundant dZn inventory
851 on seasonal timescales. Our analysis suggests that enhanced total biomass and low pCO₂ act as
852 primary influences on ρZn, and that high ρZn results in dynamic changes in the cycling of both
853 Cd and Co as a consequence of high Zn demand. Low dZn:Si slope values observed in the Ross
854 Sea and Terra Nova Bay further highlighted the intense drawdown of dZn by biota to meet a
855 high metabolic dZn demand. Overall, our study demonstrates that Zn demand is high and rapid
856 enough to depress the inventory of Zn available to phytoplankton, suggesting that Zn has been
857 overlooked as a dynamic limiting micronutrient in primary productivity modeling.
858 demonstrating strong upper water column Zn depletion. Notably, maximum Cd uptake rates
859 measured in the present study were 3.4, 3.7, and 3.3 times higher in the Amundsen Sea, Ross
860 Sea, and Terra Nova Bay, respectively, compared to the maximum Cd uptake rate of 6.1 pmol L⁻¹
861 d⁻¹ measured previously within the Costa Rica Dome using identical methods (Cox et al.,
862 2014), demonstrating the influence of high productivity and the native community on the flux of
863 dCd into the particulate phase.

864 The highly productive phytoplankton bloom documented in the study area resulted in an
865 intense algal Zn demand within the surface ocean, which we have quantified via uptake rate
866 measurements. This intense Zn demand shifted the demand for other trace metal micronutrients
867 as well, namely Cd and cobalt (Co) (Chmiel et al., 2023). Due to their similar charge and atomic

Formatted: Subscript

Formatted: Font: Italic

868 radii, Zn^{2+} , Co^{2+} and Cd^{2+} cations often share the same transporter uptake systems. An
869 organism's ability to utilize these metals as metabolic cofactors is influenced by their
870 environment and the affinity of the uptake ligands for each metal cation (Irving and Williams,
871 1953; Sunda and Huntsman, 1992). When dZn availability is low, more dCd and dCo are able to
872 bind transport ligands. Therefore, dZn concentrations and cycling can influence the cycling of
873 dCd and dCo, particularly in low dZn environments as documented for dCd in the present study.
874 The influence of dZn cycling on dCo distributions in this region was also documented for the
875 same expedition, with evidence for high rates of biological Co uptake in the Ross Sea driven by
876 dZn (and vitamin B₁₂) scarcity (Chmiel et al., 2023). The high Zn uptake rates measured in this
877 study therefore not only demonstrate a mechanism for the depletion of abundant Zn in coastal
878 areas with the potential for Zn scarcity during highly productive bloom events, but also reveal
879 dynamic changes in the cycling of Cd and Co as a consequence of high Zn demand. The notion
880 that Zn could limit primary productivity remains highly debated. Our Zn uptake data demonstrate
881 that demand is rapid enough to depress the inventory of Zn available to phytoplankton.

882

883 *Data availability*

884 CICLOPS (NBP18-01) CTD hydrography data (including pressure, temperature, total
885 dissolved oxygen, conductivity, fluorescence, and beam transmission; [https://www.bco-](https://www.bco-dmo.org/dataset-deployment/783917)
886 [dmo.org/dataset-deployment/783917](https://www.bco-dmo.org/dataset-deployment/783917)) in addition to total dissolved metal, Zn and Cd uptake rate,
887 macronutrient, and pigment datasets are available through the NSF Biological and Chemical
888 Oceanography Data Management Office (BCO-DMO) repository ([https://www.bco-](https://www.bco-dmo.org/deployment/778919)
889 [dmo.org/deployment/778919](https://www.bco-dmo.org/deployment/778919)). Underway pCO₂ data collected during cruise NBP1801 is
890 available through R2R, <https://doi.org/10.7284/139318>.

891 *Author contributions*

892 Conceptualization and analysis of the study was carried out by RMK and MAS. This work
893 was supervised by MAS and GRD. Funding was acquired by MAS and GRD. RJC and DR
894 contributed dCo data and discussion. DMM, MRM, NLS, IS, and RBD aided in sampling and data
895 collection. ~~TJH contributed to analysis and discussion. All co-authors contributed to data collection.~~
896 RMK and MAS wrote the manuscript with review and editing contributions from all co-authors.

897 *Competing interests*

898 The authors declare that they have no conflict of interest.

899 *Acknowledgements*

900 We thank the captain, crew, marine technicians, and science party of RVIB Nathaniel B.
901 Palmer for their support and contributions to the success of the NBP18-01 cruise, Joe Jennings
902 (OSU) for conducting macronutrient analyses, Lauren Lees for assistance with sampling, and
903 Natalie Cohen for assistance in operation of the seaFAST and application of the isotope dilution
904 technique.

905 *Funding*

906 National Science Foundation grant 2123055 (MAS)
907 National Science Foundation grant 2125063 (MAS)
908 National Science Foundation grant 1643684 (MAS)
909 National Science Foundation grant 1924554 (MAS)
910 National Science Foundation grant NSF-PLR 1643845 (RBD)
911 Simons Foundation (MAS)
912 National Science Foundation grant NSF-OPP 1644073 (GRD)
913 TJH acknowledges support from the Woods Hole Oceanographic Institution's *Ocean and*
914 *Climate Innovation Accelerator* program.

915 **References**

- 916 Arrigo, K. R., van Dijken, G. L., and Bushinsky, S.: Primary production in the Southern Ocean,
917 1997–2006, *Journal of Geophysical Research*, 113, C08004,
918 <https://doi.org/10.1029/2007JC004551>, 2008.
- 919 Arrigo, K. R., Lowry, K. E., and van Dijken, G. L.: Annual changes in sea ice and phytoplankton
920 in polynyas of the Amundsen Sea, Antarctica, *Deep Sea Research Part II: Topical Studies in*
921 *Oceanography*, 71–76, 5–15, <https://doi.org/10.1016/j.dsr2.2012.03.006>, 2012.
- 922 de Baar, H. J. W., Saager, P. M., Nolting, R. F., and van der Meer, J.: Cadmium versus
923 phosphate in the world ocean, *Marine Chemistry*, [https://doi.org/10.1016/0304-4203\(94\)90082-](https://doi.org/10.1016/0304-4203(94)90082-5)
924 5, 1994.
- 925 de Baar, H. J. W., van Heuven, S. M. A. C., Abouchami, W., Xue, Z., Galer, S. J. G.,
926 Rehkämper, M., Middag, R., and van Ooijen, J.: Interactions of dissolved CO₂ with cadmium
927 isotopes in the Southern Ocean, *Marine Chemistry*, 195, 105–121,
928 <https://doi.org/10.1016/J.MARCHEM.2017.06.010>, 2017.
- 929 Baars, O. and Croot, P. L.: The speciation of dissolved zinc in the Atlantic sector of the Southern
930 Ocean, *Deep Sea Research Part II: Topical Studies in Oceanography*, 58, 2720–2732,
931 <https://doi.org/10.1016/j.dsr2.2011.02.003>, 2011.
- 932 Baars, O., Abouchami, W., Galer, S. J. G., Boye, M., and Croot, P. L.: Dissolved cadmium in the
933 Southern Ocean: Distribution, speciation, and relation to phosphate, *Limnology and*
934 *Oceanography*, 59, 385–399, <https://doi.org/10.4319/LO.2014.59.2.0385>, 2014.
- 935 Bertrand, E. M., Saito, M. A., Rose, J. M., Riesselman, C. R., Lohan, M. C., Noble, A. E., Lee,
936 P. A., and DiTullio, G. R.: Vitamin B 12 and iron colimitation of phytoplankton growth in the
937 Ross Sea, *Limnology and Oceanography*, 52, 1079–1093,
938 <https://doi.org/10.4319/lo.2007.52.3.1079>, 2007.
- 939 Biller, D. V. and Bruland, K. W.: Analysis of Mn, Fe, Co, Ni, Cu, Zn, Cd, and Pb in seawater
940 using the Nobias-chelate PA1 resin and magnetic sector inductively coupled plasma mass
941 spectrometry (ICP-MS), *Marine Chemistry*, <https://doi.org/10.1016/j.marchem.2011.12.001>,
942 2012.
- 943 Bishop, J. K. B. and Wood, T. J.: Year-round observations of carbon biomass and flux variability
944 in the Southern Ocean, *Global Biogeochemical Cycles*, <https://doi.org/10.1029/2008GB003206>,
945 2009.
- 946 Bown, J., Laan, P., Ossebaar, S., Bakker, K., Rozema, P., and de Baar, H. J. W.: Bioactive trace
947 metal time series during Austral summer in Ryder Bay, Western Antarctic Peninsula, *Deep-Sea*
948 *Research Part II: Topical Studies in Oceanography*, <https://doi.org/10.1016/j.dsr2.2016.07.004>,
949 2017.
- 950 Boyle, E. A.: Cadmium: Chemical tracer of deepwater paleoceanography, *Paleoceanography*,
951 <https://doi.org/10.1029/PA003i004p00471>, 1988.

952 Boyle, E. A., Sclater, F., and Edmond, J. M.: On the marine geochemistry of cadmium, *Nature*,
953 <https://doi.org/10.1038/263042a0>, 1976.

954 Brand, L. E., Sunda, W. G., and Guillard, R. R. L.: Reduction of marine phytoplankton
955 reproduction rates by copper and cadmium, *Journal of Experimental Marine Biology and*
956 *Ecology*, [https://doi.org/10.1016/0022-0981\(86\)90205-4](https://doi.org/10.1016/0022-0981(86)90205-4), 1986.

957 Bruland, K. W., Knauer, G. A., and Martin, J. H.: Zinc in north-east Pacific water, *Nature*, 271,
958 741–743, <https://doi.org/10.1038/271741a0>, 1978.

959 Chmiel, R. J., Kell, R. M., Rao, D., Moran, D. M., DiTullio, G. R., and Saito, M. A.: Low cobalt
960 inventories in the Amundsen and Ross seas driven by high demand for labile cobalt uptake
961 among native phytoplankton communities, *Biogeosciences*, 20, 3997–4027,
962 <https://doi.org/10.5194/bg-20-3997-2023>, 2023.

963 Cox, A. D., Noble, A. E., and Saito, M. A.: Cadmium enriched stable isotope uptake and
964 addition experiments with natural phytoplankton assemblages in the Costa Rica Upwelling
965 Dome, *Marine Chemistry*, <https://doi.org/10.1016/j.marchem.2014.09.009>, 2014.

966 Crameri, F.: Scientific colour maps, , <https://doi.org/10.5281/ZENODO.1243862>, 2023.

967 Cullen, J. T.: On the nonlinear relationship between dissolved cadmium and phosphate in the
968 modern global ocean: Could chronic iron limitation of phytoplankton growth cause the kink?,
969 *Limnology and Oceanography*, 51, 1369–1380, <https://doi.org/10.4319/lo.2006.51.3.1369>, 2006.

970 Cullen, J. T. and Sherrell, R. M.: Effects of dissolved carbon dioxide, zinc, and manganese on
971 the cadmium to phosphorus ratio in natural phytoplankton assemblages, *Limnology and*
972 *Oceanography*, 50, 1193–1204, <https://doi.org/10.4319/lo.2005.50.4.1193>, 2005.

973 Cullen, J. T., Lane, T. W., Morel, F. M. M., and Sheerell, R. M.: Modulation of cadmium uptake
974 in phytoplankton by seawater CO₂ concentration, *Nature*, <https://doi.org/10.1038/46007>, 1999.

975 Cullen, J. T., Chase, Z., Coale, K. H., Fitzwater, S. E., and Sherrell, R. M.: Effect of iron
976 limitation on the cadmium to phosphorus ratio of natural phytoplankton assemblages from the
977 Southern Ocean, *Limnology and Oceanography*, <https://doi.org/10.4319/lo.2003.48.3.1079>,
978 2003.

979 Cutter, G. A. and Bruland, K. W.: Rapid and noncontaminating sampling system for trace
980 elements in global ocean surveys, *Limnology and Oceanography: Methods*,
981 <https://doi.org/10.4319/lom.2012.10.425>, 2012.

982 Das, P., Samantaray, S., and Rout, G. R.: Studies on cadmium toxicity in plants: A review,
983 [https://doi.org/10.1016/S0269-7491\(97\)00110-3](https://doi.org/10.1016/S0269-7491(97)00110-3), 1997.

984 DiTullio, G. R. and Smith, W. O.: Relationship between dimethylsulfide and phytoplankton
985 pigment concentrations in the Ross Sea, Antarctica, *Deep-Sea Research Part I*,
986 [https://doi.org/10.1016/0967-0637\(95\)00051-7](https://doi.org/10.1016/0967-0637(95)00051-7), 1995.

- 987 DiTullio, G. R., Geesey, M. E., Leventer, A., and Lizotte, M. P.: Algal pigment ratios in the Ross
988 Sea: Implications for Chemtax analysis of Southern Ocean data, 35–51,
989 <https://doi.org/10.1029/078ARS03>, 2003.
- 990 DiTullio, G. R., Garcia, N., Riseman, S. F., and Sedwick, P. N.: Effects of iron concentration on
991 pigment composition in *Phaeocystis antarctica* grown at low irradiance, *Biogeochemistry*, 83,
992 71–81, <https://doi.org/10.1007/s10533-007-9080-8>, 2007.
- 993 Fitzwater, S. E., Johnson, K. S., Gordon, R. M., Coale, K. H., and Smith, W. O.: Trace metal
994 concentrations in the Ross Sea and their relationship with nutrients and phytoplankton growth,
995 *Deep-Sea Research Part II: Topical Studies in Oceanography*, 47, 3159–3179,
996 [https://doi.org/10.1016/S0967-0645\(00\)00063-1](https://doi.org/10.1016/S0967-0645(00)00063-1), 2000.
- 997 Gerringa, L. J. A., Alderkamp, A.-C., van Dijken, G., Laan, P., Middag, R., and Arrigo, K. R.:
998 Dissolved Trace Metals in the Ross Sea, *Frontiers in Marine Science*, 7,
999 <https://doi.org/10.3389/fmars.2020.577098>, 2020.
- 1000 Giordano, R., Lombardi, G., Ciaralli, L., Beccaloni, E., Sepe, A., Ciprotti, M., and Costantini, S.:
1001 Major and trace elements in sediments from Terra Nova Bay, Antarctica, *Science of The Total*
1002 *Environment*, 227, 29–40, [https://doi.org/10.1016/S0048-9697\(98\)00402-1](https://doi.org/10.1016/S0048-9697(98)00402-1), 1999.
- 1003 Haas, C. E., Rodionov, D. A., Kropat, J., Malasarn, D., Merchant, S. S., and de Crécy-Lagard,
1004 V.: A subset of the diverse COG0523 family of putative metal chaperones is linked to zinc
1005 homeostasis in all kingdoms of life, *BMC Genomics*, 10, 470, [https://doi.org/10.1186/1471-](https://doi.org/10.1186/1471-2164-10-470)
1006 2164-10-470, 2009.
- 1007 Hopwood, M. J., Carroll, D., Höfer, J., Achterberg, E. P., Meire, L., Le Moigne, F. A. C., Bach,
1008 L. T., Eich, C., Sutherland, D. A., and González, H. E.: Highly variable iron content modulates
1009 iceberg-ocean fertilisation and potential carbon export, *Nature Communications* 2019 10:1, 10,
1010 1–10, <https://doi.org/10.1038/s41467-019-13231-0>, 2019.
- 1011 Horner, T. J., Lee, R. B. Y., Henderson, G. M., and Rickaby, R. E. M.: Nonspecific uptake and
1012 homeostasis drive the oceanic cadmium cycle, *Proceedings of the National Academy of*
1013 *Sciences*, 110, 2500–2505, <https://doi.org/10.1073/pnas.1213857110>, 2013.
- 1014 Horner, T. J., Little, S. H., Conway, T. M., Farmer, J. R., Hertzberg, J. E., Janssen, D. J., Lough,
1015 A. J. M., McKay, J. L., Tessin, A., Galer, S. J. G., Jaccard, S. L., Lacan, F., Paytan, A., Wuttig,
1016 K., and GEOTRACES–PAGES Biological Productivity Working Group Members: Bioactive
1017 Trace Metals and Their Isotopes as Paleoproductivity Proxies: An Assessment Using
1018 GEOTRACES-Era Data, *Global Biogeochemical Cycles*, 35, e2020GB006814,
1019 <https://doi.org/10.1029/2020GB006814>, 2021.
- 1020 Hutchins, D. and Bruland, K.: Grazer-mediated regeneration and assimilation of Fe, Zn and Mn
1021 from planktonic prey, *Mar. Ecol. Prog. Ser.*, 110, 259–269, <https://doi.org/10.3354/meps110259>,
1022 1994.

- 1023 Hutchins, D. A. and Bruland, K. W.: Fe, Zn, Mn and N transfer between size classes in a coastal
1024 phytoplankton community: Trace metal and major nutrient recycling compared, *issn: 0022-2402*,
1025 53, 297–313, <https://doi.org/10.1357/0022240953213197>, 1995.
- 1026 Hutchins, D. A., Wang, W. X., Schmidt, M. A., and Fisher, N. S.: Dual-labeling techniques for
1027 trace metal biogeochemical investigations in aquatic plankton communities, *Aquatic Microbial*
1028 *Ecology*, <https://doi.org/10.3354/ame019129>, 1999.
- 1029 Irving, B. H. and Williams, R. J. P.: The Stability of Transition-metal Complexes, *Journal of the*
1030 *Chemical Society (Resumed)*, <https://doi.org/10.1039/JR9530003192>, 1953.
- 1031 Jackson, S. L., Spence, J., Janssen, D. J., Ross, A. R. S., and Cullen, J. T.: Determination of Mn,
1032 Fe, Ni, Cu, Zn, Cd and Pb in seawater using offline extraction and triple quadrupole ICP-
1033 MS/MS, *Journal of Analytical Atomic Spectrometry*, 33, 304–313,
1034 <https://doi.org/10.1039/c7ja00237h>, 2018.
- 1035 Kato, T., Nakamura, S., and Morita, M.: Determination of Nickel, Copper, Zinc, Silver,
1036 Cadmium and Lead in Seawater by Isotope Dilution Inductively Coupled Plasma Mass
1037 Spectrometry, *ANAL. SCI.*, 6, 623–626, <https://doi.org/10.2116/analsci.6.623>, 1990.
- 1038 Kell, R. M., Subhas, A. V., Schanke, N. L., Lees, L. E., Chmiel, R. J., Rao, D., Brisbin, M. M.
1039 M., Moran, D. M., McIlvin, M. R., Bolinesi, F., Mangoni, O., Casotti, R., Balestra, C., Horner,
1040 T., Dunbar, R. B., Allen, A. E., DiTullio, G. R., and Saito, M. A.: Zinc stimulation of
1041 phytoplankton in a low carbon dioxide, coastal Antarctic environment,
1042 <https://doi.org/10.1101/2023.11.05.565706>, 5 November 2023.
- 1043 Kellogg, R. M., Moosburner, M. A., Cohen, N. R., Hawco, N. J., McIlvin, M. R., Moran, D. M.,
1044 DiTullio, G. R., Subhas, A. V., Allen, A. E., and Saito, M. A.: Adaptive responses of marine
1045 diatoms to zinc scarcity and ecological implications, *Nature Communications* 2022 13:1, 13, 1–
1046 13, <https://doi.org/10.1038/s41467-022-29603-y>, 2022.
- 1047 Lane, E. S., Semeniuk, D. M., Strzepek, R. F., Cullen, J. T., and Maldonado, M. T.: Effects of
1048 iron limitation on intracellular cadmium of cultured phytoplankton: Implications for surface
1049 dissolved cadmium to phosphate ratios, *Marine Chemistry*, 115, 155–162,
1050 <https://doi.org/10.1016/J.MARCHEM.2009.07.008>, 2009.
- 1051 Lane, T. W., Saito, M. A., George, G. N., Pickering, I. J., Prince, R. C., and Morel, F. M. M.: A
1052 cadmium enzyme from a marine diatom, *Nature*, 435, 42–42, <https://doi.org/10.1038/435042a>,
1053 2005.
- 1054 Latour, P., Wuttig, K., van der Merwe, P., Strzepek, R. F., Gault-Ringold, M., Townsend, A. T.,
1055 Holmes, T. M., Corkill, M., and Bowie, A. R.: Manganese biogeochemistry in the Southern
1056 Ocean, from Tasmania to Antarctica, *Limnology and Oceanography*, 66, 2547–2562,
1057 <https://doi.org/10.1002/lno.11772>, 2021.
- 1058 Lee, J. and Morel, F.: Replacement of zinc by cadmium in marine phytoplankton, *Marine*
1059 *Ecology Progress Series*, 127, 305–309, <https://doi.org/10.3354/meps127305>, 1995.

1060 Lee, J. G., Roberts, S. B., and Morel, F. M. M.: Cadmium: A nutrient for the marine diatom
1061 *Thalassiosira weissflogii*, *Limnology and Oceanography*,
1062 <https://doi.org/10.4319/lo.1995.40.6.1056>, 1995.

1063 Lohan, M. C., Statham, P. J., and Crawford, D. W.: Total dissolved zinc in the upper water
1064 column of the subarctic North East Pacific, *Deep Sea Research Part II: Topical Studies in*
1065 *Oceanography*, 49, 5793–5808, [https://doi.org/10.1016/S0967-0645\(02\)00215-1](https://doi.org/10.1016/S0967-0645(02)00215-1), 2002.

1066 Martin, J. H.: Glacial-interglacial CO₂ change: The Iron Hypothesis, *Paleoceanography*,
1067 <https://doi.org/10.1029/PA005i001p00001>, 1990.

1068 Middag, R., Baar, H. J. W., and Bruland, K. W.: The relationships between dissolved zinc and
1069 major nutrients phosphate and silicate along the GEOTRACES GA02 transect in the West
1070 Atlantic Ocean, *Global Biogeochemical Cycles*, 33, 63–84,
1071 <https://doi.org/10.1029/2018GB006034>, 2019.

1072 Morel, F. M. M., Reinfelder, J. R., Roberts, S. B., Chamberlain, C. P., Lee, J. G., and Yee, D.:
1073 Zinc and carbon co-limitation of marine phytoplankton, *Nature*, 369, 740–742,
1074 <https://doi.org/10.1038/369740A0>, 1994.

1075 Morel, F. M. M., Milligan, A. J., and Saito, M. A.: Marine Bioinorganic Chemistry: The Role of
1076 Trace Metals in the Oceanic Cycles of Major Nutrients, in: *Treatise on Geochemistry: Second*
1077 *Edition*, <https://doi.org/10.1016/B978-0-08-095975-7.00605-7>, 2013.

1078 Morel, F. M. M., Lam, P. J., and Saito, M. A.: Trace metal substitution in marine phytoplankton,
1079 *Annual Review of Earth and Planetary Sciences*, 48, 491–517, [https://doi.org/10.1146/annurev-](https://doi.org/10.1146/annurev-earth-053018-060108)
1080 [earth-053018-060108](https://doi.org/10.1146/annurev-earth-053018-060108), 2020.

1081 Noble, A. E., Lamborg, C. H., Ohnemus, D. C., Lam, P. J., Goepfert, T. J., Measures, C. I.,
1082 Frame, C. H., Casciotti, K. L., DiTullio, G. R., Jennings, J., and Saito, M. A.: Basin-scale inputs
1083 of cobalt, iron, and manganese from the Benguela-Angola front to the South Atlantic Ocean,
1084 *Limnology and Oceanography*, <https://doi.org/10.4319/lo.2012.57.4.0989>, 2012.

1085 Noble, A. E., Moran, D. M., Allen, A. E., and Saito, M. A.: Dissolved and particulate trace metal
1086 micronutrients under the McMurdo Sound seasonal sea ice: basal sea ice communities as a
1087 capacitor for iron, *Frontiers in Chemistry*, 1, <https://doi.org/10.3389/fchem.2013.00025>, 2013.

1088 Ohnemus, D. C., Rauschenberg, S., Cutter, G. A., Fitzsimmons, J. N., Sherrell, R. M., and
1089 Twining, B. S.: Elevated trace metal content of prokaryotic communities associated with marine
1090 oxygen deficient zones, *Limnology and Oceanography*, <https://doi.org/10.1002/lno.10363>, 2017.

1091 Oldham, V. E., Chmiel, R., Hansel, C. M., DiTullio, G. R., Rao, D., and Saito, M.: Inhibited
1092 Manganese Oxide Formation Hinders Cobalt Scavenging in the Ross Sea, *Global*
1093 *Biogeochemical Cycles*, 35, <https://doi.org/10.1029/2020GB006706>, 2021.

1094 Park, H., Song, B., and Morel, F. M. M.: Diversity of the cadmium-containing carbonic
1095 anhydrase in marine diatoms and natural waters, *Environmental Microbiology*,
1096 <https://doi.org/10.1111/j.1462-2920.2006.01151.x>, 2007.

- 1097 Park, H., McGinn, P. J., and Morel, F. M. M.: Expression of cadmium carbonic anhydrase of
1098 diatoms in seawater, *Aquatic Microbial Ecology*, <https://doi.org/10.3354/ame01192>, 2008.
- 1099 Person, R., Vancoppenolle, M., Aumont, O., and Malsang, M.: Continental and Sea Ice Iron
1100 Sources Fertilize the Southern Ocean in Synergy, *Geophysical Research Letters*, 48,
1101 e2021GL094761, <https://doi.org/10.1029/2021GL094761>, 2021.
- 1102 Planquette, H., Sherrell, R. M., Stammerjohn, S., and Field, M. P.: Particulate iron delivery to the
1103 water column of the Amundsen Sea, Antarctica, *Marine Chemistry*, 153, 15–30,
1104 <https://doi.org/10.1016/j.marchem.2013.04.006>, 2013.
- 1105 Price, N. M. and Morel, F. M. M.: Cadmium and cobalt substitution for zinc in a marine diatom,
1106 *Nature*, 344, 658–660, <https://doi.org/10.1038/344658a0>, 1990.
- 1107 Rapp, I., Schlosser, C., Rusiecka, D., Gledhill, M., and Achterberg, E. P.: Automated
1108 preconcentration of Fe, Zn, Cu, Ni, Cd, Pb, Co, and Mn in seawater with analysis using high-
1109 resolution sector field inductively-coupled plasma mass spectrometry, *Analytica Chimica Acta*,
1110 <https://doi.org/10.1016/j.aca.2017.05.008>, 2017.
- 1111 Rudge, J. F., Reynolds, B. C., and Bourdon, B.: The double spike toolbox, *Chemical Geology*,
1112 <https://doi.org/10.1016/j.chemgeo.2009.05.010>, 2009.
- 1113 Saito, M. A. and Goepfert, T. J.: Zinc-cobalt colimitation of *Phaeocystis antarctica*, *Limnology*
1114 *and Oceanography*, 53, 266–275, <https://doi.org/10.4319/lo.2008.53.1.0266>, 2008.
- 1115 Sedwick, P. N., Di Tullio, G. R., and Mackey, D. J.: Iron and manganese in the Ross Sea,
1116 Seasonal iron limitation in Antarctic, *Journal of Geophysical Research: Oceans*,
1117 <https://doi.org/10.1029/2000JC000256>, 2000.
- 1118 Sedwick, P. N., Marsay, C. M., Sohst, B. M., Aguilar-Islas, A. M., Lohan, M. C., Long, M. C.,
1119 Arrigo, K. R., Dunbar, R. B., Saito, M. A., Smith, W. O., and DiTullio, G. R.: Early season
1120 depletion of dissolved iron in the Ross Sea polynya: Implications for iron dynamics on the
1121 Antarctic continental shelf, *Journal of Geophysical Research*, 116, C12019,
1122 <https://doi.org/10.1029/2010JC006553>, 2011.
- 1123 Shaked, Y., Xu, Y., Leblanc, K., and Morel, F. M. M.: Zinc availability and alkaline phosphatase
1124 activity in *Emiliana huxleyi*: Implications for Zn-P co-limitation in the ocean, *Limnology and*
1125 *Oceanography*, 51, 299–309, <https://doi.org/10.4319/lo.2006.51.1.0299>, 2006.
- 1126 Sieber, M., Conway, T. M., de Souza, G. F., Hassler, C. S., Ellwood, M. J., and Vance, D.:
1127 Cycling of zinc and its isotopes across multiple zones of the Southern Ocean: Insights from the
1128 Antarctic Circumnavigation Expedition, *Geochimica et Cosmochimica Acta*,
1129 <https://doi.org/10.1016/j.gca.2019.09.039>, 2020.
- 1130 Sohrin, Y., Urushihara, S., Nakatsuka, S., Kono, T., Higo, E., Minami, T., Norisuye, K., and
1131 Umetani, S.: Multielemental determination of GEOTRACES key trace metals in seawater by
1132 ICPMS after preconcentration using an ethylenediaminetriacetic acid chelating resin, *Analytical*
1133 *Chemistry*, <https://doi.org/10.1021/ac800500f>, 2008.

- 1134 St-Laurent, P., Yager, P. L., Sherrell, R. M., Stammerjohn, S. E., and Dinniman, M. S.: Pathways
1135 and supply of dissolved iron in the Amundsen Sea (Antarctica), *Journal of Geophysical*
1136 *Research: Oceans*, 122, 7135–7162, <https://doi.org/10.1002/2017JC013162>, 2017.
- 1137 Sunda, W. G. and Huntsman, S. A.: Feedback interactions between zinc and phytoplankton in
1138 seawater, *Limnology and Oceanography*, 37, 25–40, <https://doi.org/10.4319/lo.1992.37.1.0025>,
1139 1992.
- 1140 Sunda, W. G. and Huntsman, S. A.: Cobalt and zinc interreplacement in marine phytoplankton:
1141 Biological and geochemical implications, *Limnology and Oceanography*, 40, 1404–1417,
1142 <https://doi.org/10.4319/lo.1995.40.8.1404>, 1995.
- 1143 Sunda, W. G. and Huntsman, S. A.: Antagonisms between cadmium and zinc toxicity and
1144 manganese limitation in a coastal diatom, *Limnology and Oceanography*, 41, 373–387,
1145 <https://doi.org/10.4319/lo.1996.41.3.0373>, 1996.
- 1146 Sunda, W. G. and Huntsman, S. A.: Control of Cd Concentrations in a Coastal Diatom by
1147 Interactions among Free Ionic Cd, Zn, and Mn in Seawater, *Environmental Science &*
1148 *Technology*, 32, 2961–2968, <https://doi.org/10.1021/es980271y>, 1998a.
- 1149 Sunda, W. G. and Huntsman, S. A.: Processes regulating cellular metal accumulation and
1150 physiological effects: Phytoplankton as model systems, *Science of The Total Environment*, 219,
1151 165–181, [https://doi.org/10.1016/S0048-9697\(98\)00226-5](https://doi.org/10.1016/S0048-9697(98)00226-5), 1998b.
- 1152 Sunda, W. G. and Huntsman, S. A.: Effect of Zn, Mn, and Fe on Cd accumulation in
1153 phytoplankton: Implications for oceanic Cd cycling, *Limnology and Oceanography*, 45, 1501–
1154 1516, <https://doi.org/10.4319/lo.2000.45.7.1501>, 2000.
- 1155 Tan, D., Xu, W., Zhu, Z., Li, S., Wu, G., and Qin, H.: Optimizing the ratio of the spike to sample
1156 for isotope dilution analysis: a case study with selenium isotopes, *Acta Geochimica*,
1157 <https://doi.org/10.1007/s11631-019-00390-6>, 2020.
- 1158 Taylor, S. R. and McLennan, S. M.: *The Continental Crust: Its Composition and Evolution.*,
1159 Blackwell Scientific Publications, Oxford, 312 pp., 1985.
- 1160 Twining, B. S. and Baines, S. B.: The trace metal composition of marine phytoplankton., *Annual*
1161 *review of marine science*, 5, 191–215, <https://doi.org/10.1146/annurev-marine-121211-172322>,
1162 2013.
- 1163 Vance, D., Little, S. H., De Souza, G. F., Khatiwala, S., Lohan, M. C., and Middag, R.: Silicon
1164 and zinc biogeochemical cycles coupled through the Southern Ocean, *Nature Geoscience*, 10,
1165 202–206, <https://doi.org/10.1038/NGEO2890>, 2017.
- 1166 Weber, T., John, S., Tagliabue, A., and DeVries, T.: Biological uptake and reversible scavenging
1167 of zinc in the global ocean, *Science*, 361, 72–76, <https://doi.org/10.1126/SCIENCE.AAP8532>,
1168 2018.

- 1169 Wright, S. W., van den Enden, R. L., Pearce, I., Davidson, A. T., Scott, F. J., and Westwood, K.
1170 J.: Phytoplankton community structure and stocks in the Southern Ocean (30-80°E) determined
1171 by CHEMTAX analysis of HPLC pigment signatures, *Deep-Sea Research Part II: Topical*
1172 *Studies in Oceanography*, <https://doi.org/10.1016/j.dsr2.2009.06.015>, 2010.
- 1173 Wu, J. and Boyle, E. A.: Determination of iron in seawater by high-resolution isotope dilution
1174 inductively coupled plasma mass spectrometry after Mg(OH)₂ coprecipitation, *Analytica*
1175 *Chimica Acta*, 367, 183–191, [https://doi.org/10.1016/S0003-2670\(98\)00145-7](https://doi.org/10.1016/S0003-2670(98)00145-7), 1998.
- 1176 Wuttig, K., Townsend, A. T., van der Merwe, P., Gault-Ringold, M., Holmes, T., Schallenberg,
1177 C., Latour, P., Tonnard, M., Rijkenberg, M. J. A., Lannuzel, D., and Bowie, A. R.: Critical
1178 evaluation of a seaFAST system for the analysis of trace metals in marine samples, *Talanta*,
1179 <https://doi.org/10.1016/j.talanta.2019.01.047>, 2019.
- 1180 Xu, Y., Tang, D., Shaked, Y., and Morel, F. M. M.: Zinc, cadmium, and cobalt interreplacement
1181 and relative use efficiencies in the coccolithophore *Emiliana huxleyi*, *Limnology and*
1182 *Oceanography*, 52, 2294–2305, <https://doi.org/10.4319/lo.2007.52.5.2294>, 2007.
- 1183 Zhao, Y., Vance, D., Abouchami, W., and de Baar, H. J. W.: Biogeochemical cycling of zinc and
1184 its isotopes in the Southern Ocean, *Geochimica et Cosmochimica Acta*,
1185 <https://doi.org/10.1016/j.gca.2013.07.045>, 2014.
- 1186